European Commission

JRC SCIENCE AND POLICY REPORTS

Cerium Dioxide, NM-211, NM-212, NM-213. Characterisation and test item preparation

JRC Repository: NM-series of Representative Manufactured Nanomaterials

Charanjeet Singh, Steffi Friedrichs, Giacomo Ceccone, Neil Gibson, Keld Alstrup Jensen, Marcus Levin, Heidi Goenaga Infante, David Carlander and Kirsten Rasmussen

2014

Report EUR 26649 EN

European Commission
Joint Research Centre
Institute for Health and Consumer Protection

Contact information
IHCP Communication Office
Address: Joint Research Centre, Via Enrico Fermi 2749, 21027 Ispra (VA), Italy
E-mail: jrc-ihcp-communication@ec.europa.eu
Tel.: +39 0332 78 9618
Fax: +39 0332 78 5388

https://ec.europa.eu/jrc

JRC89825

EUR 26649 EN

ISBN 978-92-79-38308-3 (PDF)
ISBN 978-92-79-38309-0 (print)

ISSN 1831-9424 (online)
ISSN 1018-5593 (print)

Doi:10.2788/80203

Luxembourg: Publications Office of the European Union, 2014

Abstract

In 2011 the JRC launched a repository for Representative Nanomaterials to support both EU and international research projects, and especially the OECD Working Party on Manufactured Nanomaterials that leads an exploratory programme "Testing a Representative set of Manufactured Nanomaterials", aiming to generate and collect data on characterisation and (eco)toxicological properties to understand relevant end-points as well as the applicability of OECD Test Guidelines for testing nanomaterials. The Repository responds to a need for nanosafety research purposes: availability of nanomaterial from a single production batch to enhance the comparability of results between different research laboratories and projects.

The present report presents the physico-chemical characterisation of the manufactured nano cerium dioxide, NM-211 and NM-212 from the JRC repository, both originating from a single batch of commercially manufactured material. In addition data on a bulk (i.e. macro-sized) CeO_2, NM-213, is included, which also originates from a single batch; NM-213 is not in the JRC repository.

The studies were performed in close collaboration between the PROSPEcT project, where the partners are the Fraunhofer Institute for Molecular and Applied Ecology (Fh-IME, Germany), LGC standards (United Kingdom), the National Research Centre for the Working Environment (NRCWE, Denmark), Commonwealth Scientific and Industrial Research Organisation (CSIRO, Australia) and the National Measurement Institute of Australia. In addition, the JRC contributed study results to the characterisation of the materials.

JRC Repository: NM-Series of Representative Manufactured Nanomaterials

Cerium Dioxide, NM-211, NM-212, NM-213. Characterisation and test item preparation

Charanjeet Singh
Nanotechnology Industries Association, London, United Kingdom

Steffi Friedrichs, David Carlander
Nanotechnology Industries Association, Brussels, Belgium

Marcus Levin, Keld Alstrup Jensen
The National Research Centre for the Working Environment, DK-2100 Copenhagen, Denmark

Heidi Goenaga Infante
Laboratory of the Government Chemist, LGC standards, United Kingdom

Kirsten Rasmussen, Neil Gibson, Giacomo Ceccone
European Commission, Joint Research Centre, Institute for Health and Consumer Protection, 21027 Ispra (VA), Italy

Abstract

The European Commission's Joint Research Centre (JRC) provides scientific support to European Union (EU) policy regarding nanotechnology. Within this context, the European Commission's Joint Research Centre launched, in February 2011, a repository for Representative Test Materials (RTMs), based on preparatory work started in 2008. The repository supports both EU and international research projects, and especially the OECD Working Party on Manufactured Nanomaterials (WPMN). The WPMN leads an exploratory testing programme "Testing a Representative set of Manufactured Nanomaterials" for the development and collection of data on characterisation, toxicological and ecotoxicological properties, as well as risk assessment and safety evaluation of nanomaterials. One important purpose is to understand the applicability of the OECD Test Guidelines for the testing of nanomaterials as well as end-points relevant for such materials.

The Repository responds to a nanosafety research need, which is the availability of nanomaterial from a single production batch to enhance the comparability of results between different research laboratories and projects. The availability of representative nanomaterials to the international scientific community enhances and enables development of safe materials and products.

The present report presents the physico-chemical characterisation of Representative Test Materials of manufactured nano cerium dioxide, NM-211 and NM-212, and the bulk NM-213, each originating from a single batch of commercially manufactured material. The materials were tested for the OECD test programme "Testing a representative set of manufactured nanomaterials". NM-213 is included in the series as a bulk comparator. The CeO_2 NMs may be used as representative material in the measurement and testing with regard to hazard identification, risk and exposure assessment studies.

The results for 15 physico-chemical endpoints are addressed in the present report, including size and size distribution, crystallite size and electron microscopy images, zeta potential and dispersibility, and sample and test item preparation procedures.

The studies were performed with the PROSPEcT project[1], where the partners are the Fraunhofer Institute for Molecular and Applied Ecology (Fh-IME, Germany), LGC standards (United Kingdom), the National Research Centre for the Working

[1] http://www.nanotechia.org/activities/prospect-ecotoxicology-test-protocols-representative-nanomaterials-support-oecd

Environment (NRCWE, Denmark), Commonwealth Scientific and Industrial Research Organisation (CSIRO, Australia) and the National Measurement Institute of Australia. In addition, the JRC contributed study results to the characterisation of the materials.

Table of contents

List of abbreviations

APS	Aerodynamic Particle Sizer
BAM	Federal Institute for Materials Research and Testing, Germany
BET	Brunauer–Emmett–Teller (BET) theory aims to explain the physical adsorption of gas molecules on a solid surface. It serves as the basis for an important analysis technique to measure the specific surface area of a material
BSA	Bovine Serum Albumin
CEN	Comité Européen de Normalisation
CLS	Centrifugal Liquid Sedimentation
COV	Calculated coefficient of variation
CRM	Certified Reference Material
DI	De-ionised (water)
DLS	Dynamic Light Scattering
FMPS	Fast Mobility Particle Size
GDMF	General Decision Making Framework
GLP	Good Laboratory Practice
Fh-IME	Fraunhofer Institute for Molecular Biology and Applied Ecology, Germany
HEPA	High-Efficiency Particulate Air (filter)
IHCP	Institute for Health and Consumer Protection (European Commission)
ISO	International Organisation for Standardization
IUPAC	International Union of Pure and Applied Chemistry
JRC-IHCP	Joint Research Centre (European Commission)
LDE	Laser Doppler Electrophoresis
MNP	Manufactured NanoParticle
NIST	National Institute of Science and Technology, USA
NM	Nanomaterial
OECD	Organisation for Economic Co-operation and Development
PROSPEcT	Ecotoxicology Test Protocols for Representative Nanomaterials in Support of the OECD Sponsorship Programme'.
RH	Relative Humidity
RM	Reference Material
RMN	Representative Manufactured Nanomaterial
ROS	Reactive Oxygen Species
RSD	Relative Standard Deviation
RTM	Representative Test Material
SD	Standard Deviation
SEM	Scanning Electron Microscopy
SMPS	Scanning Mobility Particle Sizer
SSA	Specific Surface Area
SOP	Standard Operating Procedure
TEM	Transmission Electron Microscopy
UV-VIS	Ultraviolet-visible Spectrophotometry
WPMN	Working Party on Manufactured Nanomaterials
w/w%	Weight percent
XRD	X-Ray Diffraction

1 Introduction – Cerium Dioxide

Nanotechnology holds considerable promise in many technological areas and industrial sectors and the application of nanosciences and nanostructured materials to everyday products offers a range of benefits. Their application in every-day consumer products may make these lighter, stronger, cleaner, less expensive, more efficient, more precise, more functional, more durable, and also more aesthetic. Products with specific properties derived from nanotechnology currently available on the market include for example textiles, cosmetics and beauty products, water filters, food, food-packaging materials, paints, glues and dental fillers. Nanomaterials may also improve our quality of life via their use in applications leading to more efficacious pharmaceuticals, improved medical diagnostic tools and faster computers, to name but a few. This has been matched by growth in requests for characterised representative nanomaterials for use as reference matrices for testing to reliably address health and safety issues for humans and the environment related to nanomaterials and corresponding implementation of European policy and responsible nanotechnology decisions (Morris *et al.* 2011, Ju-Nam *et al.* 2008).

Nanoparticles can be naturally occurring or manufactured; they can be classed into several categories, which include the following (Chandra Ray *et al.* 2009):

1. Metal nanomaterials, such as gold and silver nanoparticles
2. Metal oxide nanomaterials, such as titanium dioxide and zinc oxide
3. Carbon nanomaterials such as fullerenes and nanotubes
4. Quantum dots such as cadmium telluride and cadmium selenide

One estimate for the production of engineered nanomaterials was 2000 tonnes in 2004 and increasing to 58,000 tonnes by 2011-2020 (Nowack *et al.* 2007).

For nanosafety research purposes, the availability of nanomaterial from a single batch is desirable to enhance the comparability of results between different laboratories and research projects. The availability of such materials would overcome questions related to whether a nanomaterial tested in one project is the same or just similar to a nanomaterial tested in other projects and how results compare. In response to this need as well as supporting the OECD Working Party on Manufactured Nanomaterials (WPMN) programme for "Testing a Representative set of Manufactured Nanomaterials" (the WPMN Testing Programme) the European Commission's Joint Research Centre (JRC) established a repository with Representative Test Materials (RTMs) hosting

different types of nanomaterials. The role of Representative Test Materials is described in a recent publication (Roebben *et al*., 2013).

PROSPEcT[2] is UK's contribution to the WPMN Testing Programme and it examines the environmental safety of nanomaterials in accordance with the OECD WPMN 'Guidance Manual for the Testing of Manufactured Nanomaterials: OECD's Sponsorship Programme' (OECD 2010a). PROSPEcT partnership states regarding the PROSPEcT project:

"It will provide crucial data to the OECD work, by addressing gaps in the current level of knowledge on the physico-chemical and ecotoxicological properties of these materials, followed by fundamental scientific research leading to establishing scientific test methodologies to study those endpoints that may not be assessed through standard tests used for bulk chemicals. Manufactured Nanoparticles (MNP) are characterised by specific properties which are "engineered" into the structure of the particle. MNP potentially offer many economic, environmental and technological advantages. However, there is concern that the properties engineered into MNP may represent risks to the environment if MNP are released in an uncontrolled fashion into the environment. PROSPEcT will specifically provide crucial data for the future development, manufacture and commercialisation of products containing nanoparticles of cerium oxide and zinc oxide, but more generally help to support advancement and commercialisation of a broad group of nanomaterials. PROSPEcT started on 1st January 2009 and was completed in 2012."

This report focuses on cerium dioxide (CeO_2) NMs. Commercially CeO_2 has numerous applications including petroleum refining (cracking catalyst), polishing agent (for glass mirrors, plate glass, television tubes, ophthalmic lenses, precision optics, electronic wafers), coatings and fuel cells. CeO_2 is applied in a variety of consumer products including semiconductors and as an additive in cigarettes. CeO_2 nanoparticles are mainly employed as diesel fuel additive, designed to increase fuel combustion efficiency and decrease diesel soot emissions by performing as a combustion catalyst (HEI Report 2001; Cassee *et al.* 2011). Despite the efficient trapping of particulate matter (soot), engine tests have shown that a small amount of CeO_2 is emitted in the particulate phase exhaust. CeO_2 detected in diesel exhaust emissions employing nanoscale cerium based fuel additive was found to be in the nanoscale (Cassee *et al.* 2011). The potential

[2] **PROSPEcT: Ec**otoxicology **T**est **P**rotocols for **R**epresentative Nanomaterials in Support of the **O**ECD **S**ponsorship **P**rogramme'. For further information, please visit http://www.nanotechia.org/activities/prospect-ecotoxicology-test-protocols-representative-nanomaterials-support-oecd

environmental and health effects associated with the use, including use as diesel fuel additive, of CeO_2 nanoparticles are not known.

Currently, metal oxide nanoparticles have not been comprehensively assessed in regard to potential effects on human health, from exposure (accidental or otherwise) in the workplace during nanoparticles production or exposure through use in commercial products, or for their effects on ecosystems if released into the environment. However, the potential of any material to induce adverse effects on health and the environment depends both on the biological toxicity associated with the material (hazard) and on the level of exposure. The risk posed by a material may change during its lifecycle from manufacture through to its demise or transformation into other forms (Osmond *et al.* 2010).

The two CeO_2 nanomaterials NM-211 and NM-212 were introduced by the JRC to be studied in the OECD Testing Programme. The Fraunhofer Institute introduced NM-213 as CeO_2 bulk representative material. In the OECD WPMN Testing Programme NM-211 and NM-212 are the principle materials.

The present report describes a number of physico-chemical properties that have been measured for the CeO_2 NMs reflecting end-points in the OECD WPMN Testing Programme. More than 15 endpoints are addressed, including size and size distribution, crystallite size and electron microscopy images. Sample and test item preparation procedures are addressed as well. The results are based on studies by several laboratories as well as by the JRC. (The authors would like to acknowledge the contribution of F. Pianella, JRC, of Figure 7 to Figure **10**).

2 Overview of the JRC NM-Series of Representative Test Materials

The JRC established the JRC Nanomaterials Repository for the NM-series of Representative Test Materials in 2011, and it is hosted at the Institute for Health and Consumer Protection in Italy (IHCP).

Table 1. List of representative Nanomaterials in the JRC NM Repository (2013).

NM code	Type of material*	Label name	Other information
NM-100	**Titanium Dioxide**	**Titanium Dioxide**	
NM-101	Titanium Dioxide	Titanium Dioxide	anatase
NM-102	Titanium Dioxide	Titanium Dioxide, anatase	anatase
NM-103	Titanium Dioxide	Titanium Dioxide thermal, hydrophobic	rutile
NM-104	Titanium Dioxide	Titanium Dioxide thermal, hydrophilic	rutile
NM-105	Titanium Dioxide	Titanium Dioxide rutile-anatase	anatase-rutile
NM-110	**Zinc Oxide, uncoated**	**Zinc Oxide**	
NM-111	Zinc Oxide, coated	Zinc Oxidecoatedtriethoxycaprylsilane	
NM-200	**Silicon Dioxide**	**Synthetic Amorphous Silica PR-A-02**	**precipitated**
NM-201	Silicon Dioxide	Synthetic Amorphous Silica PR-B-01	precipitated
NM-202	Silicon Dioxide	Synthetic Amorphous Silica PY-AB-03	thermal
NM-203	Silicon Dioxide	Synthetic Amorphous Silica PY-A-04	thermal
NM-204	Silicon Dioxide	Synthetic Amorphous Silica PR-A-05	precipitated
NM-211	**Cerium Dioxide**	**Cerium (IV) Oxide precipitated, uncoated, cubic**	
NM-212	Cerium Dioxide	Cerium (IV) Oxide precipitated, uncoated	
NM-300K	**Silver**	**Silver<20 nm**	
NM-300K DIS	Silver - dispersant	Ag - dispersant	
NM-330	**Gold**		
NM-330 DIS	Gold - dispersant	Gold - dispersant	
NM-400	**MWCNT**	**Multi-walled Carbon Nanotubes**	
NM-401	MWCNT	Multi-walled Carbon Nanotubes	
NM-402	MWCNT	Multi-walled Carbon Nanotubes	
NM-403	MWCNT	Multi-walled Carbon Nanotubes	
NM-600	**Nanoclay**	**Bentonite**	

* Nanomaterials, even of the same chemical composition, may be available e.g. in various sizes and/or shapes, which may influence their chemical and physical properties

Currently, the Repository contains eight of the nanomaterial chemistries tested in the OECD WPMN Testing Programme and a total of 22 representative nanomaterials, see Table 1. The chemistries are titanium dioxide, zinc oxide, silicon dioxide, cerium dioxide, silver, gold, multi-walled carbon nanotubes and bentonite (a nanoclay). Furthermore, the dispersants for silver and gold are also available from the repository. The sub-sampling was done in collaboration with the Fraunhofer Institute for Molecular Biology and Applied Ecology, and each nanomaterial was homogenised and sub-sampled into vials under reproducible (GLP) conditions. Each nanomaterial in the Repository originates from a

random single industrial production batch, produced within industrial specifications. Thus, to the extent feasible for industrial materials, all sub-samples from one material should be identical and differences in test results between laboratories for the same end-point should not be attributed to differences in the material tested. The nanomaterials were allocated an identifying code with the following format: the letters "NM" followed by a dash and three digits (NM-XXX), the NM-series. In 2014 the code format was changed to JRCNM<5digit number><letter><six digit number>. The <5 digit number> identifies the material, the <letter> identifies the batch of origin and the <6 digit number> is the unique vial number for that batch.

The materials are studied in projects investigating properties of nanomaterials at all levels of co-operation: national, European and global. More than 10,000 individual vials have been distributed to research institutions, national authorities, industrial research laboratories and other scientific stakeholders in the EU, Switzerland, USA, Canada, Australia, China, Russia, Japan, and Korea.

Study results for the WPMN Testing Programme are collated in a JRC database, JRC NANOhub, and are made available to the OECD through access to the JRC NANOhub. The combination of availability of representative test nanomaterials and data in the JRC NANOhub builds a foundation for research and product development, thus supporting innovation and competitiveness for nanotechnology industries.

2.1 Representativeness of the Materials in the NM-series

To reliably address the scientific questions concerning nanomaterial induced effects for toxicity, ecotoxicity and environmental fate and behaviour, it is important to study representative test nanomaterials that are relevant for industrial application and commercial use, and for which a critical mass of study results are available. Representative test materials allow enhanced comparison of test results, robust assessment of data, and pave the way for appropriate test method optimisation, harmonisation and validation and may finally serve as performance standards for testing.

In the following, the concept of Representative Test Material (RTM) is briefly outlined clarifying the difference to reference materials. Reference Material (RM) is the generic name for materials that have a proven and sufficient homogeneity and stability in terms of a defined intended use, and for certified reference materials (CRM) there is a certified value for the property of interest. RMs and CRMs need to be produced and used applying the conditions and terms standardised and described in ISO Guides 30 to 35 relating to reference material production. Currently, only a small number of certified

reference materials exist in the field of manufactured nanomaterials, for example gold nanoparticles (certified size) and single-wall carbon nanotube soot (certified composition) from the USA National Institute of Standards and Technology (NIST), silver nanoparticles (certified size) from the German Federal Institute for Materials Research and Testing (BAM) and colloid silica (certified size) from the JRC Institute for Reference Materials and Measurements (IRMM).

The nanomaterials in the JRC repository are representative test materials. For RTMs the following definition was proposed by Roebben et al. (2013):

> *A **representative test material (RTM)** is a material from a single batch, which is sufficiently homogeneous and stable with respect to one or more specified properties, and which implicitly is assumed to be fit for its intended use in the development of test methods which target properties other than the properties for which homogeneity and stability have been demonstrated.*

An RTM is not a reference material for the tests for which it is intended to be used, because homogeneity and stability are not demonstrated for the corresponding measurand. However, an RTM is more valuable than an ordinary test material, since it has been checked for homogeneity and stability in terms of one or more specified properties. RTMs are extremely useful tools in intra- or interlaboratory development of methods for which reference materials are not (yet) available. Thus, the NM-series of representative test materials are complementary to (certified) Reference Materials as illustrated in Table 2.

Table 2: Comparison of the essential characteristics of the concept 'representative test material' to the concepts of 'reference material' and 'certified reference material'.

	Representative Test Material	**Reference Material**	
		Not certified	**Certified**
Parent material	Representative for a class of materials to be investigated with the target method(s)		
Homogeneity / stability	Assumed for the measurands of interest, demonstrated for other measurands	Demonstrated for the measurands of interest	Demonstrated for the measurands of interest
Assigned property value	None	None, or indicative only.	Certified for the measurand of interest

The OECD WPMN uses the term “Representative Manufactured Nanomaterial” for the nanomaterials selected for testing, which are assumed to be representative for a large fraction of nanomaterials on the market.

2.2 The OECD WPMN and Testing the NM-series

In 2006 international recognition of the need of a deeper understanding of nanomaterials, including relevant characterisation information as well as hazard profiles of nanomaterials led to the establishment of the WPMN under the Chemicals Committee of the OECD. The WPMN leads one of the most comprehensive nanomaterial research programmes "Safety Testing of a Set of Representative Manufactured Nanomaterials", established in 2007. The deadline for submitting the dossiers for the OECD WPMN was 21 June 2013.

The WPMN agreed on a list of Representative Manufactured Nanomaterials to be tested and relevant end-points to test for exploratory purposes. The nanomaterials listed in the testing programme are (2012): fullerenes, single-wall and multi-wall carbon nanotubes, cerium dioxide, zinc oxide, iron oxide, gold, silver, titanium dioxide, silicon dioxide, nanoclay and dendrimers. Some of these materials are hosted in the JRC Repository.

Data in the OECD testing programme regarding characterisation, toxicological and eco-toxicological effects are generated in Phase 1, see Table 3, to understand the hazard profiles of the nanomaterials. A Phase 2 is planned and will start by evaluating the data received in Phase 1, and especially the test guidelines applied to identify their applicability and necessary modifications (if any). Then the need for further testing, as relevant, will be considered. The Guidance Manual for the Testing of Manufactured Nanomaterials (OECD 2010a, OECD 2010b) describes in detail the information expectations for each end-point and all end-points have to be addressed.

Table 3. Endpoints agreed by the OECD WPMN for the Representative Manufactured Nanomaterials.

Nanomaterial Information / Identification		**Environmental fate**	
1	Nano material name	27	Dispersion stability in water
2	CAS number	28	Biotic degradability
3	Structural formula / molecular structure	29	- Ready biodegradability
4	Composition of NM being tested (incl. degree of purity, known impurities or additives)	30	- Simulation testing on ultimate degradation in surface water
5	Basic Morphology	31	- Soil simulation testing
6	Description of surface chemistry (e.g. coating or modification)	32	- Sediment simulation testing
7	Major commercial uses	33	- Sewage treatment simulation testing
8	Known catalytic activity	34	Identification of degradation product(s)
9	Method of production (e.g. precipitation, gas phase)	35	Further testing of degradation product(s) as required
Physical-chemical Properties and Material Characterization		36	Abiotic degradability and fate
10	Agglomeration / aggregation	37	- Hydrolysis, for surface modified nanomaterials
11	Water solubility	38	Adsorption - desorption
12	Crystalline phase	39	Adsorption to soil or sediment
13	Dustiness	40	Bioaccumulation potential
14	Crystallite size	41	Bioaccumulation in sediment
15	Representative TEM picture(s)	**Environmental toxicology**	
16	Particle size distribution	42	Effects on pelagic species (short/ long term)
17	Specific surface area	43	Effects on sediment species (short/ long term)
18	Zeta potential (surface charge)	44	Effects on soil species (short/ long term)
19	Surface chemistry (where appropriate)	45	Effect on terrestrial species
20	Photo-catalytic activity	46	Effect on micro-organisms
21	Pour density (must be completed)	47	Other relevant information
22	Porosity	**Mammalian toxicology**	
23	Octanol-water partition coefficient, where relevant	48	Pharmacokinetics (ADME)
24	Redox potential	49	Acute Toxicity
25	Radical formation	50	Repeated dose toxicity
26	Other relevant information (where available)	IF AVAILABLE	
		51	Chronic toxicity
Material safety		52	Reproductive toxicity
57	Flammability	53	Developmental toxicity
58	Explosivity	54	Genetic toxicity
59	Incompatibility	55	Experience with human exposure
		56	Other relevant test data

In addition to the listed endpoints in the Guidance Manual for Sponsors (GMS), the GMS advises (p. 25): "To aid in assuring the identical nature of the sponsored MN, the material used in different tests should be obtained preferably in a single lot, and stored and manipulated in comparable, if not identical procedures." and further "Sponsors will identify the source of test nanomaterials, including all known aspects of material production, the

manufacturer, facility location, lot number, and any other pertinent information as noted in Annex I "Nanomaterial Information/Identification"." Thus, the GMS recommends ensuring that, as far as possible, the testing of all endpoints is performed with a nanomaterial from one batch. The JRC repository materials fulfil this.

The provision of the JRC NM-Series to the OECD WPMN testing programme enables the development of the comprehensive data set on characterisation nanomaterial properties and toxicological and ecotoxicological behaviour, as described above. In 2012 the OECD WPMN recommended the development of a risk assessment/safety evaluation methodology for nanomaterials, based on, among others, this data set.

2.3 Characterisation of the NM-series

For nanomaterials it is known that their hazardous properties can be affected by for example shape, size and surface area, because these parameters affect the transport properties of the particles (absorption, distribution, and excretion).

In addition, one of the issues raised consistently in the discussions under the OECD WPMN for nanomaterials evaluation is the "test item" preparations and dispersion protocols. A "test item" is simply (the actual fraction of) the sample tested. This discussion is linked to the characterisation of the nanomaterials for which a number of relevant scenarios have been identified, and among these are:

Characterisation

I. as received
II. as dispersed
III. during testing

These scenarios reflect that many of the nanomaterials tested are insoluble (in water and other media) or only slightly soluble nanoparticles, and their physico-chemical properties as well as their (eco)toxicological effects are closely linked also to their physical surroundings. Thus, to acquire an in-depth understanding of the nanomaterials, material characterisation should be performed for a number of the different stages of the nanomaterials' use cycle. Table 3, sections "nanomaterial information" and "physico-chemical properties", list the characterisation end-points. Most of these may be measured both for the dry material and in dispersion; however, obviously some belong to a specific preparation form for the measurement: dustiness is a dry measurement whereas the water/octanol coefficient can be measured only in solution. Additional issues could be relevant, e.g. if the physical state and preparation of the material tested is representative for production and use, taking into account the chain of actors and life cycle.

Below is described a number of issues to consider for the characterisation.

I. "as received" is the characterisation of the properties of a RTM as received, and typical preparations are dry or aqueous.

II and III. "as dispersed" and **"during testing"** are for the nanomaterials undergoing further sample preparation steps, which should be assessed with regard to influence on measurement results, such as particle size determinations for the different scenarios: dry material, in aqueous or physiological media.

In addition to the physico-chemical characterisation, also data relating to (eco)toxicological effects are requested in the OECD Test Programme. For this kind of testing, the test item preparation needs to be carefully considered. The characterisation of matrix-dependent properties of the prepared test item is an important issue for nanomaterials. Results are dependent on the matrix composition and protocols used. Chapter 4 describes the PROsPECT dispersion protocol and lists some protocols from EU projects.

For the testing, RTMs can best be used and brought into a matrix under defined conditions and applying defined procedures, and availability of protocols also for the matrices should minimise sources of uncertainties and methodological errors. Thus, dispersion protocols have been developed for test item preparation for use in test systems for (eco)toxicological testing or environmental fate analysis, comprising conditioning and choice of matrix components. Hence, the prepared test item should fulfil the requirements of the test method under GLP conditions and be representative for the selected exposure route. Test items are prepared for environmental testing in the compartments soil, water, sediment, sewage treatment plants as well as for oral, dermal, (intravenous) and inhalation toxicity testing, in the form it is assumed to reach the biological entity in the test system.

Depending on the various protocols used, different results may be obtained for the same parameter measured. Also the effect of the 'corona' of a particle, i.e. the molecules surrounding it in a given medium, has been acknowledged (Cedervall et al., 2007), emphasising that the constituents of the corona depend on the medium. Biophysical characterisation, such as corona composition, kinetics/exchange rates, corona structure and depletion effects/changes in matrix kinetics are therefore required in support of understanding of test items.

The determination of a property should be addressed by the selection of the appropriate measurand and the corresponding measurement method. For nanomaterials the "appropriate measurand" is not yet fully understood for all endpoints, and extensive discussion and guidance development take place in several international fora: the Scientific Committee on Emerging and Newly Identified Health Risks (SCENIHR 2009), the OECD WPMN, the Comité Européen de Normalisation Technical Committee 352 (CEN/TC 352), Nanotechnologies, and the International Standardisation Organisation (ISO) under Technical Committee 229 (ISO/TC 229), Nanotechnologies. In addition, for the measurements an uncertainty estimate should be described based on the Guide for Uncertainty in Measurements.

3 NM characterisation

The first part of this section describes the characteristics of the CeO_2 as in the repository i.e. as delivered. The physico-chemical endpoints are listed in Table 3 and described in the Guidance Manual for Sponsors (OECD, 2010a), and Table 4 gives an overview of the characterisation performed and the institutions involved.

Table 4. Physico-chemical characterisation performed, and institutions involved.

Physico-chemical Properties and Material Characterization	NM characterised			Method	Institutions(s)
	211	212	213		
Agglomeration/aggregation	x	x	x	TEM	CSIRO
	x	x	x	DLS	CSIRO
	x	x	x	SEM	CSIRO, NPL
	x	x	x	CLS	NPL
Water solubility[1]	x			Turbidity	NPL
	x	x	x	Flask method	CSIRO, NPL
		x	x	Dialysis	CSIRO
Crystalline phase	x	x	x	XRD	CSIRO, DEAKIN, JRC
Dustiness	x	x	x	Rotating cylinder	NPL
Crystallite size	x	x	x	XRD	CSIRO, NPL, DEAKIN, JRC
Representative TEM picture(s)	x	x	x	TEM	CSIRO, NMI, DEAKIN, NPL, INIA
Particle size distribution	x	x	x	SEM	NPL
	x	x	x	DLS	NPL, INIA, CSIRO
	x	x	x	SMPS	NPL
	x	x	x	TEM	NMI, NPL, INIA
	x	x	x	CPS	NPL
Specific surface area (SSA)	x	x	x	BET	NPL, INIA, CSIRO, DEAKIN, JRC
Zeta potential (surface charge)	x	x	x	LDE	NPL, CSIRO
	x	x	x	DLS	INIA
Surface chemistry (where appropriate)	x	x		XPS	NPL, CSIRO, JRC
Presence of coating	Measurement not performed				
Photo-catalytic activity	x	x	x	UV-vis Spectroscopy	NPL, DEAKIN, CSIRO
Pour density	x	x	x	Tapped density	NPL
Porosity	x	x	x	BET	CSIRO, NPL
Octanol-water partition coefficient, where relevant	Endpoint not relevant				
Redox potential	x	x	x	ORP	NPL
OH radical formation, acellular	x	x	x	UV-vis Spectroscopy	NPL

[1] Turbidity measurements of dispersion stabilities in Di water, Fish medium, sea water and daphnia medium, US EPA Medium

For selected properties, a specific vehicle or media need to be used for sample preparation to perform the measurement. The relevant endpoints are listed as part of Table 3 and are described in the Guidance Manual for Sponsors.

When testing the NMs, up to 4 different media were applied for dispersing the nanomaterials: De-Ionized (DI) water, Fish medium, Seawater and Daphnia medium. DI water is simply di-ionized water. The Fish medium, Seawater medium and Daphnia medium are three types of ecotoxicology relevant media, and were prepared as follows:

a) Seawater, in which 25 g per L of Tropic Marine Sea Salt (Tropical and Marine Limited), were made up resulting in pH ~ 8.8.

b) Daphnia freshwater media. This was prepared by firstly dissolving appropriate salts (196 mg $CaCl_2$•$2H_2O$, 82 mg $MgSO_4$•$7H_2O$, 65 mg $NaHCO_3$, 0.002 mg Na_2SeO_3 (as obtained by appropriate dilutions of a 2 mg/ml stock solution)) in 1 L of DI water. Upon continued stirring, DI water was further added so that conductivity was between ~ 360 – 480 µS/cm. End volume ~ 1 – 1.5 L. Final pH ~ 7.9.

c) Fish freshwater media. This was prepared in three separate steps. Firstly, salts (11.76 g $CaCl_2$•$2H_2O$, 4.93 g $MgSO_4$•$7H_2O$, 2.59 g $NaHCO_3$, 0.23 g KCl) were dissolved separately in 1L of DI water to make four separate stock solutions. Secondly, 25 mL of each salt stock solution was aliquot into a clean bottle and diluted in DI water (made up to 1 L volume). Thirdly, 200 ml of the stock solution from Step 2 was aliquoted and further diluted with DI water (made up to 1L volume). Final pH ~ 7.3.

In the following sections the results of the testing performed is described end-point by end-point.

3.1 Agglomeration/aggregation

3.1.1 Scanning Electron Microscopy (SEM)

3.1.1.1 Method

A Philips XL30 field emission Scanning Electron Microscope (SEM) was used for this study. The optimal spatial resolution of the microscope was from 2-5 nm with varying accelerating voltage from 30 KV to 1 kV. Images of CeO_2 particles were acquired at an accelerating voltage of 5 kV, a working distance of ≈ 10 mm, and a tilt angle 0°.

An SEM metal stub was covered with adhesive conducting tape and a small amount of "as received" CeO_2 powder (around 5 mg) was sprinkled over the tape. The surface of the powder sample was flattened with a spatula. Excess powder was removed by gently tapping the stub on its side until a light coating of powder on the surface became apparent. The nanoparticles were thinly sputtered with iridium using a Polaron SC570 sputter coater. Ar sputtering was conducted under vacuum. The coating deposition time was 20 seconds at a plate current of 50mA, giving a coating thickness of approximately 1 nm.

3.1.1.2 Results

Figures 1, 2 and 3 provide typical SEM images of NM-211, NM-212 and NM-213. The SEM images reveal that "as received" CeO_2 particles are highly agglomerated. The particle size is smallest for NM-211 and largest for NM-213; NM-213 is "bulk" CeO_2 so it is expected to have the largest of the three materials.

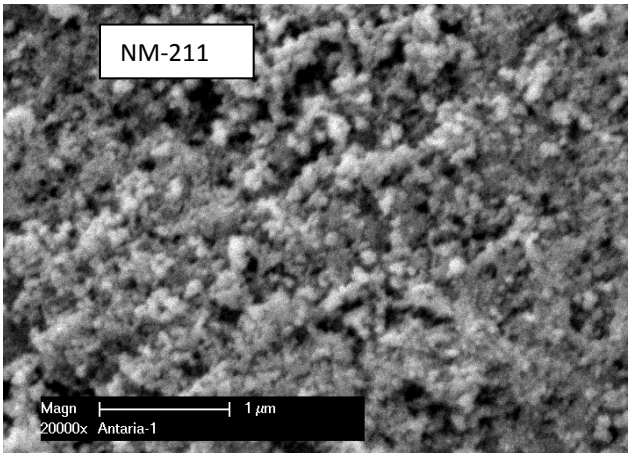

Figure 1. SEM image of NM-211, indicating high agglomeration of particles.

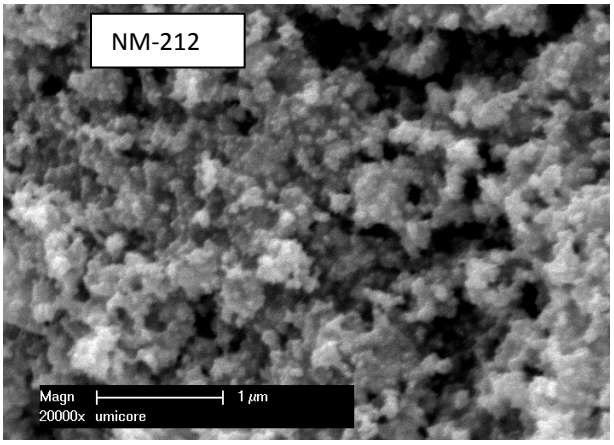

Figure 2. SEM image of NM-212, indicating high agglomeration of particles.

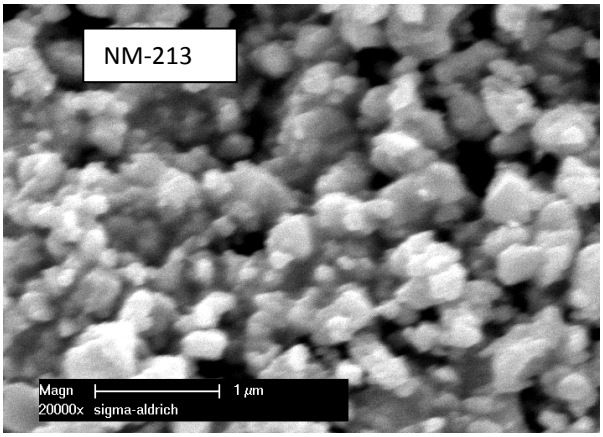

Figure 3. SEM image of NM-213 indicating high agglomeration of particles.

3.1.2 Dynamic Light Scattering

Dynamic Light Scattering (DLS) is a technique to characterise colloidal systems based on the scattering of visible light resulting from the difference in refractive index between the dispersed colloids and the dispersion medium. DLS may be applied for sizing particles in the range from ca. 0.6 nm to ca. 6 μm depending on the optical properties of the material and medium. In DLS, the transmitted or back-scattered light from a laser diode is measured as function of time. A photo-detector collects the signal, which will fluctuate with time depending on the level of Brownian motion of the suspended nm- to µm-size objects in liquid suspension. The Brownian motion is caused by collision between the particle and the molecules of the medium and varies as a function of particle size and causes variation in the intensity of transmitted or scattered light as function of time. A correlator compares the signal measured at a time t_0 with different, very short time delays *dt* (autocorrelation). As the particles move, the correlation between t_0 and subsequent *dt* signals decreases with time, from a perfect correlation at t_0, to a complete decorrelation at infinite time (in practice order of milliseconds). For large particles, the signal changes slowly and the correlation persists for a long time, whereas small particles have high Brownian movement causing rapid decorrelation.

DLS measurement results should be interpreted carefully, as the performance of the DLS method and instrumentation may be limited for measurements on mixtures of particles of different sizes. DLS measurements on the single components of one well-defined size gave results corresponding to the findings obtained by using TEM, however the measurement results regarding the size distribution of mixtures of such components showed significant limitations, e.g. the smaller particles were not identified by the measured distribution (Calzolai *et al*., 2011; Linsinger *et al.*, 2012).

3.1.2.1 Method

Measurements of hydrodynamic size were obtained using a Brookhaven particle size analyzer 90Plus equipped with a 657 nm laser. Reference standards (Duke polystyrene latex, standards (Duke polystyrene latex, with a nominal size of 100 nm, and NIST RM8013 Au nanoparticles with a nominal size of 60 nm) were used to assess the performance of the instrument. 10 mg “as received” CeO_2 particles were added to a measuring cuvette containing 3 ml of deionised water. The cuvette was placed in an ultrasonic bath, ultrasonicated for 10 seconds and then shaken to ensure the particles were well dispersed before starting the dynamic light scattering measurements. Each size distribution curve and correlation function curve that was generated was based on

10 measurements. Experiments for each sample were performed in triplicate. The temperature was maintained at 25°C. The cuvette was thoroughly washed with deionised water after each experiment.

3.1.2.2 Results

Figures 4, 5 and 6 show size distribution curves and correlation function curves for NM-211, NM-212 and NM-213 obtained from three individual runs.

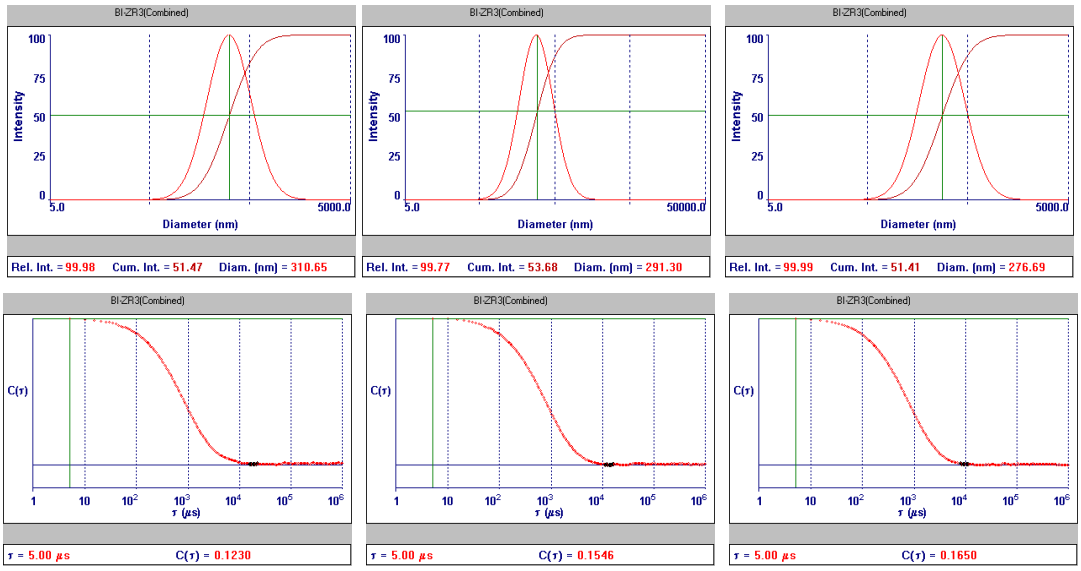

Figure 4. Size distribution curves and correlation function curves for NM-211 (mean hydrodynamic size 293 nm, mean polydispersity 0.304).

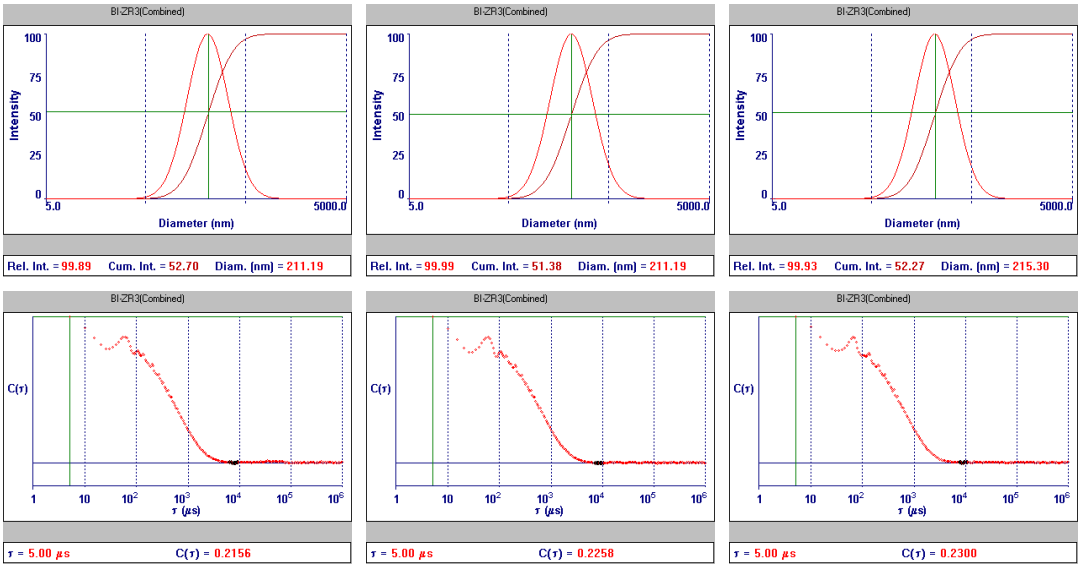

Figure 5. Size distribution curves and correlation function curves for NM-212 (mean hydrodynamic size 213 nm, mean polydispersity 0.255).

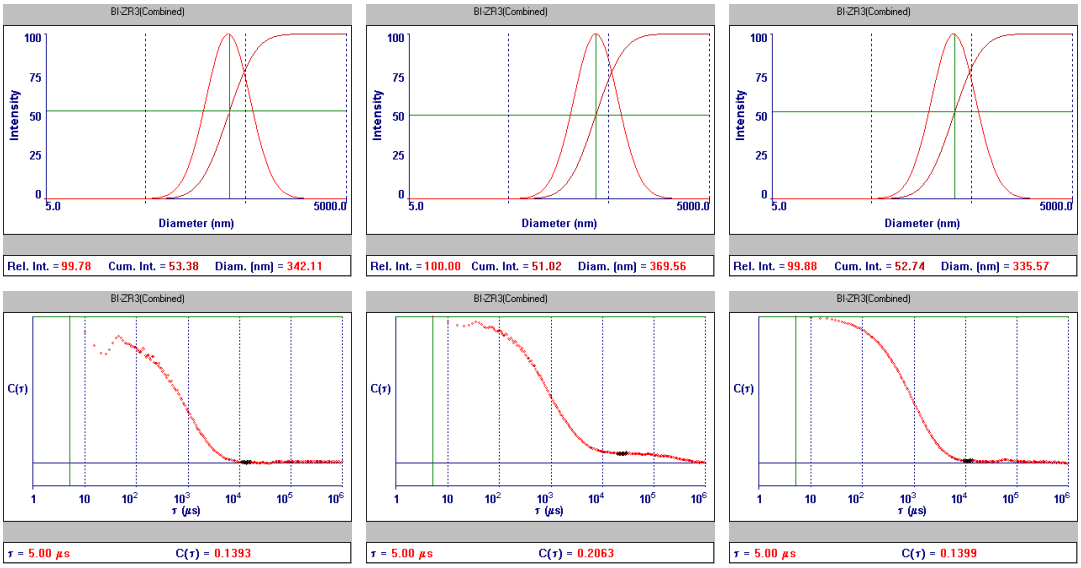

Figure 6. Size distribution curves and correlation function curves for NM-213 (mean hydrodynamic size 349 nm, mean polydispersity 0.300).

The mean hydrodynamic sizes for NM-211, NM-212 and NM-213 are 293 nm, 213 nm and 349 nm respectively. These hydrodynamic diameters appear to be independent of the primary particle sizes, suggesting that particles from all CeO_2 NMs are aggregated / agglomerated when dispersed in DI water. The results show that NM-211, NM-212 and NM-213 are all relatively polydisperse.

3.1.2.3 Results from the JRC

The JRC characterised NM-211 and NM-212 by DLS (Dynamic Light Scattering). NM-211 and NM-212 were dispersed in MilliQ water (1 mg/ml) and then sonicated using Vial Tweeter sonicator (Hielscher Ultrasound technology, Vial Tweeter UIS250v) for 15 minutes (cycle = 0.5; amplitude 75). Samples were then immediately analysed DLS (Malvern Instruments, Zetasizer Nano series, Nano – ZS).

The results of the DLS measurements were very diverse, and may be explained, to a large extent, by the measurement principle of the DLS technique, see section 3.1.2.1. Figure 7 and Figure 8 show typical measurement curves from the DLS analysis of NM-211 and NM-212. As the DLS measurement is based on the intensity of back scattered light from each particle and that is inversely proportional to the sixth power of the nanoparticle radius, even just a few large particles will “cover” the signal from the smaller ones. Thus, the DLS technique is recommended for characterization of (known) monodisperse materials; however this is not the case for NM-211 and NM-212 from the JRC Repository, and in general the mean particle diameter from DLS analysis tend to be bigger than the one resulting from CLS analysis.

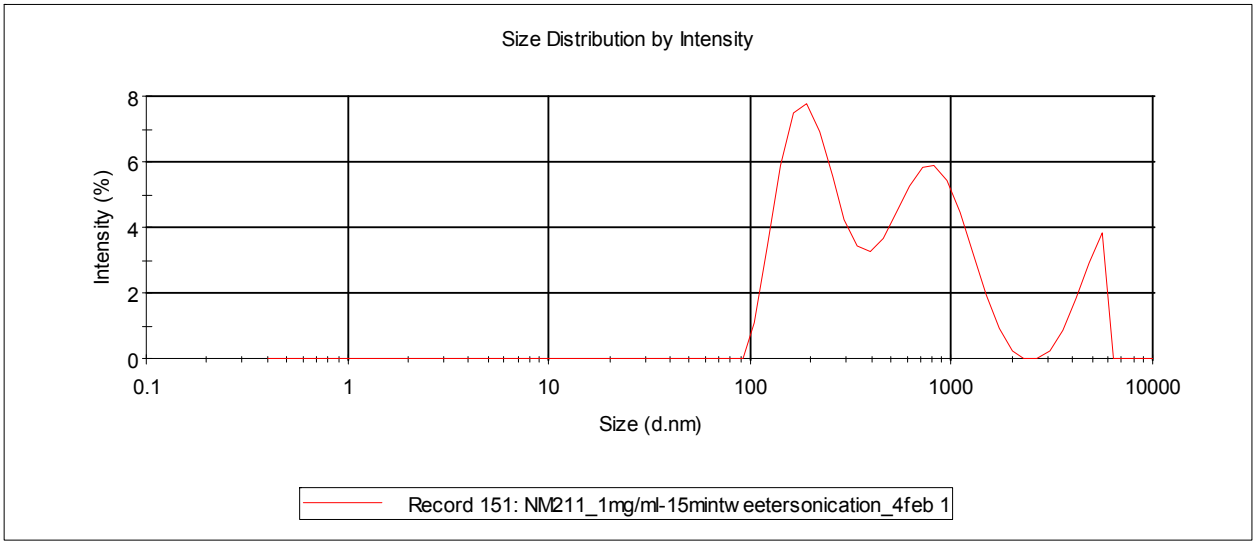

Figure 7. DLS size distribution curve for NM-211.

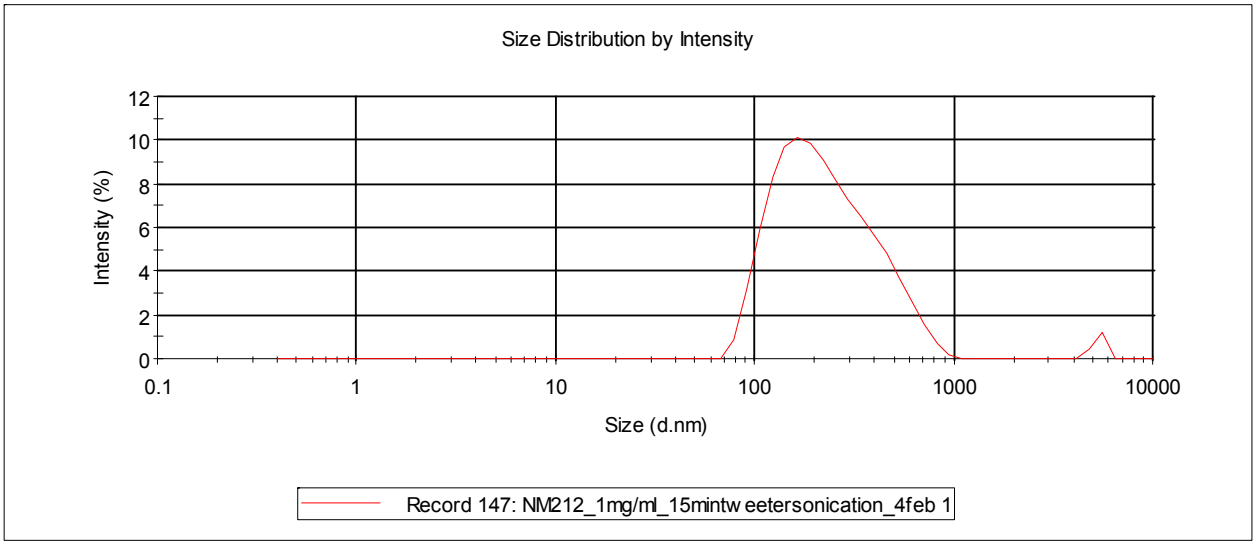

Figure 8. DLS size distribution curve for NM-212.

3.1.3 Centrifugal Liquid Sedimentation Disc Centrifuge

3.1.3.1 Method

Particle size distribution by centrifugal liquid sedimentation (CLS) technique was measured using a CPS Disc Centrifuge Model DC 20000 instrument (Analytik Ltd, UK). At the start of the method, the centrifuge was brought up to speed by partially filling the disc with a sucrose gradient fluid and dodecane cap fluid. The purpose of the gradient fluid was to stabilise the sedimentation; the purpose of the cap fluid was to maintain the gradient inside the disc. The disc centrifuge was then allowed to equilibrate at 6000 rpm for 1 hour; this gradient will be stable and used within the next 6 hours. 0.2 ml of the nanoparticle sample (50 mg/L) was injected into the disc; a calibration standard was injected after every three samples. Analysis was run against a calibration standard, NIST traceable standard, PVC 0.377 micron. The Disc Centrifuge Control System software (CPS Instruments Inc.) was used to acquire and process the data.

When analysing the results it must be emphasized that the values for NP sizes obtained by CLS correspond to the nominal density of CeO_2. In reality, since the particles are agglomerated, the apparent density of the aggregates is lower than the nominal density, resulting in an underestimation of the size measured.

3.1.3.2 Results, PROsPECT

Table 5 and Table 6 show the CLS disc centrifugal sedimentation results, with Table 5 showing the equivalent spherical mean particle diameter and Table 6 the corresponding D_{10}, D_{50}, D_{90} values (oversize percentiles). D_{10}, D_{50}, D_{90} values are often used to describe the particle size distribution of the sample.

Table 5. Particle size measurements by CLS disc centrifuge. The equivalent spherical particle diameter as measured by CLS centrifugal sedimentation; the mean and ± SD of 3 replicates are shown.

Material	DI water (nm)	Fish medium (nm)	Seawater (nm)	Daphnia (nm)
NM-211	340 ± 50	380 ± 50	520 ± 90	400 ± 30
NM-212	135 ± 4	164 ± 8	188 ± 2	146 ± 5
NM-213	570 ± 80	530 ± 30	650 ± 80	630 ± 40

If D_{10} = 1225 nm, then this means that that 10 mass % of the particles will have particle diameter of 1225 nm or larger. Results from Table 5 show that the largest mean particle size exists when the NMs are dispersed in seawater; this is reflected by the particle mean size as well as the corresponding D_{90} values. Results also show that the smallest

particle size exists when the NMs are dispersed in DI water, and the data suggests that larger agglomerates exist in the three ecotoxicology media, with the largest agglomerates found in seawater.

Table 6. Particle size measurement by CLS disc centrifuge. The corresponding D_{10}, D_{50}, D_{90} values (oversize percentiles) from the averaged CLS measurements.

Material	DI water (nm)	Fish medium (nm)	Seawater (nm)	Daphnia (nm)
NM-211	D_{10} 810 ± 160 D_{50} 202 ± 17 D_{90} 130 ± 60	D_{10} 900 ± 200 D_{50} 231 ± 17 D_{90} 113 ± 4	D_{10} 900 ± 500 D_{50} 400 ± 110 D_{90} 163 ± 14	D_{10} 980 ± 80 D_{50} 230 ± 20 D_{90} 108 ± 3
NM-212	D_{10} 185 ± 2 D_{50} 109 ± 3 D_{90} 73 ± 3	D_{10} 226 ± 9 D_{50} 134 ± 6 D_{90} 89 ± 5	D_{10} 521 ± 3 D_{50} 150 ± 1 D_{90} 98 ± 2	D_{10} 200 ± 5 D_{50} 90 ± 60 D_{90} 81 ± 2
NM-213	D_{10} 1110 ± 150 D_{50} 510 ± 90 D_{90} 158 ± 12	D_{10} 1060 ± 60 D_{50} 470 ± 40 D_{90} 138 ± 6	D_{10} 1160 ± 120 D_{50} 590 ± 70 D_{90} 210 ± 20	D_{10} 1210 ± 60 D_{50} 570 ± 40 D_{90} 163 ± 13

3.1.3.3 Results, JRC

The JRC characterised NM-211 and NM-212 by CLS (Centrifugal Liquid Sedimentation). NM-211 and NM-212 were dispersed in MilliQ water (1 mg/ml) and then sonicated using Vial Tweeter sonicator (Hielscher Ultrasound technology, Vial Tweeter UIS250v) for 15 minutes (cycle = 0.5; amplitude 75). Samples were then immediately analysed by CLS (CPS Instruments, Inc. CPS Disc Centrifuge, Model DC24000UHR).

Figure 9 and Figure 10 illustrate typical resulting output curves of the CLS analyses performed on NM-211 and NM-212. Results from CLS showed a mean particle size of about 126 nm for NM-211 and 112 nm for NM-212, and were the same for analyses repeated at different dates.

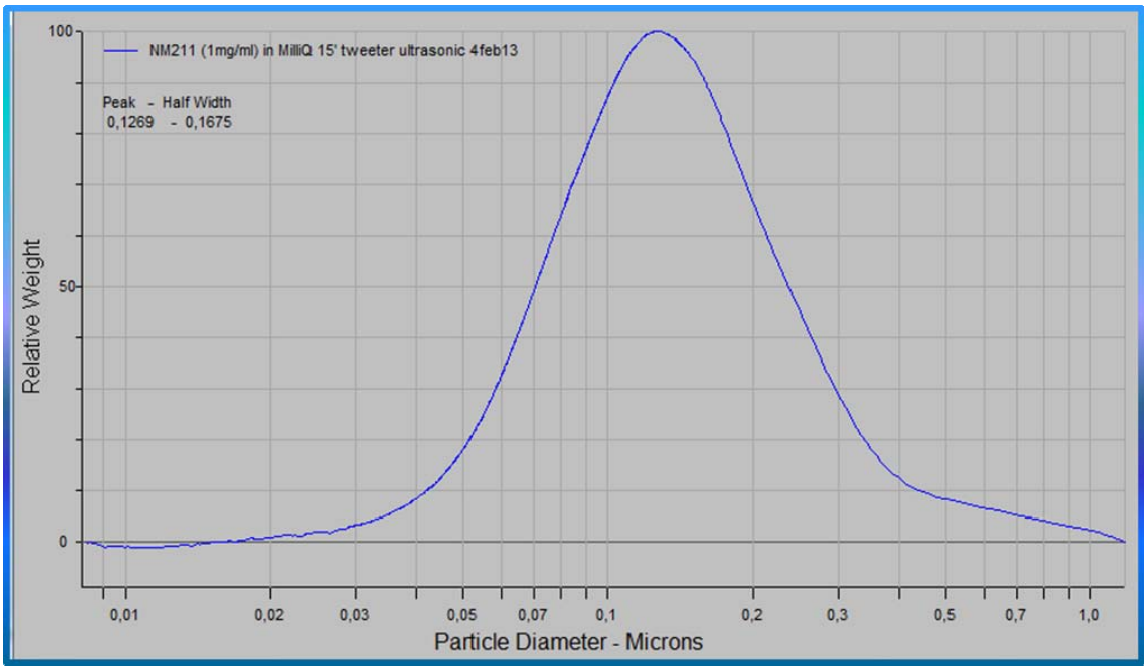

Figure 9. CLS results for NM-211.

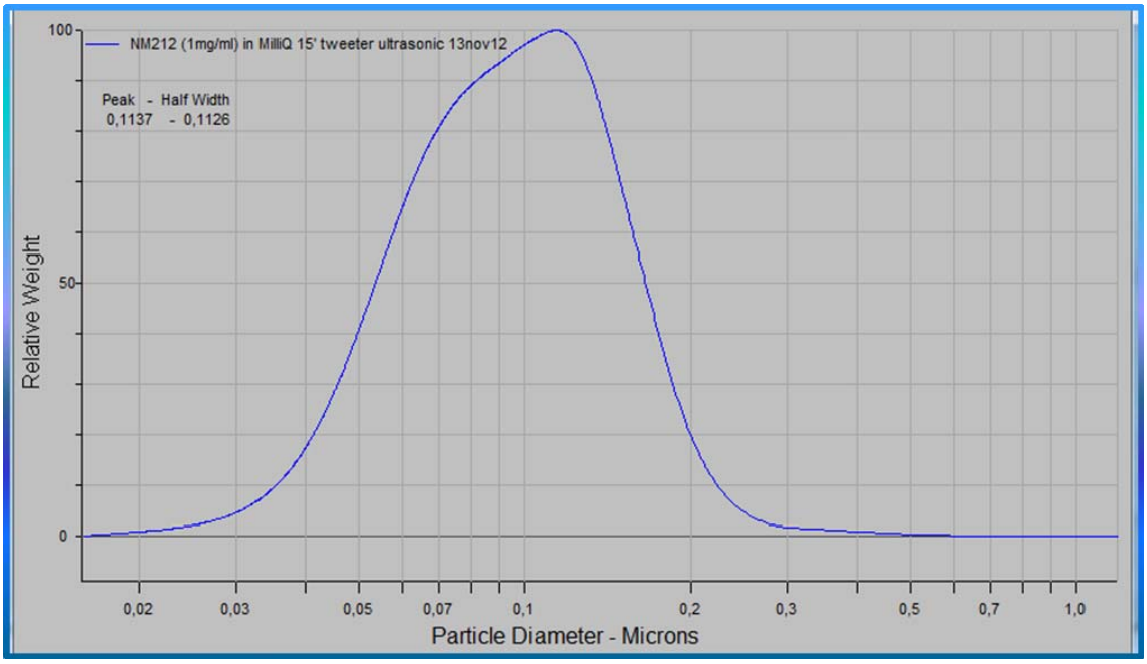

Figure 10. CLS results for NM-212.

3.1.4 Turbidity Measurements

3.1.4.1 Method

Turbidity was measured using HF Scientific – Micro100 RI turbidity meter (Cole-Palmer, UK); this meter has an infrared light source that meets the ISO standard 7027 for turbidity measurements. The meter was calibrated with standards based on AMCO-AEPA-1 microspheres; these standards are traceable to standard formazine suspension used in turbidity measurements. Standard values of 1000, 10 and 0.02 NTU (Nephelometric Turbidity Units) were used to calibrate the meter. Prior to use, the meter was allowed to warm up for 30 minutes. Sample cuvettes (HF Scientific, USA) were used to hold the sample. Note that glass thickness may vary from cuvette to cuvette and within the same cuvette. Hence, individual vials were indexed; indexing of the cuvette entails finding the point of the cuvette that light passes through that gives the lowest reading; once indexed the holder can be marked accordingly. Prior to their use, cuvettes were cleaned, in accordance to manufacturer's instructions. This involved washing the interior and exterior of the cuvette with a detergent (2% Hellmanex in DI water); it was then rinsed several times in distilled water before finally rinsing in DI water. The cuvette was further rinsed with the sample two times before filling (30ml) and analysed. The cuvette was placed into the meter and signal allowed to settle before taking readings.

3.1.4.2 Results

Table 7 shows the corresponding "half-lives" of the NM powders when dispersed in the various media. The concept of "half-lives" has been put forward in the OECD guidance manual for the testing of manufactured nanomaterial and this value is an indication of dispersion stability through time i.e. the larger the half-life value the longer it takes for the concentration to reduce by half and thus the more stable the dispersion.

Results show that overall NMs are more stable when dispersed in DI water compared to an ecotoxicology media. Also, when dispersed in DI water, NM-213 (i.e. the bulk CeO_2) results show that it is the least stable CeO_2 NM (as reflected by the small half-life value) relative to NM-211 and NM-212; this dispersion instability is also reflected by the rather small corresponding zeta-potential results. Dispersion of NM-213 in DI water was more stable compared to fish medium as seen from the half-life results. However, this finding was not consistent with the corresponding zeta-potential results, in which the dispersion was more stable in fish medium (i.e. -22 mV) when compared to DI water (i.e. –7 mV). A likely explanation for this discrepancy is that dispersion stability was measured in two

different ways i.e. through the measurement of interparticle force (zeta-potential) or through analysing the stability via sedimentation measurements (turbidity with time). The former measurement will solely be governed by the electric properties of solid surface in contact with liquid which will subsequently contribute towards sedimentation rate; the latter measurement will not only be determined by the zeta-potential value but also by other factors e.g. particle size; the larger particles will be expected to sediment faster.

Table 7. Dispersion stability (half life) in different media as measured by turbidity measurements.

Material	DI water (min)	Fish media (min)	Seawater (min)	Daphnia media (min)
NM-211	780	438	534	600
NM-212	2676	282	288	252
NM-213	432	348	294	294

3.2 Water Solubility/Dispersability

3.2.1 Dispersion Method

Dispersion was performed in accordance with the recommended PROSPEcT protocol: http://www.nanotechia.org/sites/default/files/files/PROSPECT_Disper_sion_Protocol.pdf. Concentration of 50 mg/L was achieved for each sample; a total volume of 1 L was made and stored in clean media (1 L) bottles at room temperature. After day 2, the bottles were stored in a fridge. Several extractions from the 1 L sample were made over a period of 22 days; prior to extraction, the bottles were gently agitated (this was done by hand) to allow proper mixing to ensure homogeneity. The extracted sample (~ 50 ml) was then subjected to a three-step process in order to remove particles and to extract the resultant supernatant. This step was done immediately after extraction. First step involved the extraction of aggregates/agglomerates using filtration method, through a Millipore Express PES membrane, 0.1 µm pore size filter (Fisher, UK) under vacuum. In the second step, the resulting filtrant was centrifuged (Centrifuge 5430, Eppendorf, UK) (7500 rpm for one hour). Finally, the extraction of the clear supernatant was carried out by using Peri-Star Pro peristaltic pump (World Precision Instruments, UK); this was done carefully (so as to not disturb the pellet). Less than half of the supernatant was collected. The resulting supernatant was stored in the freezer for analysis using ICP-MS.

The ICP-MS analysis was carried out using an Agilent 7500ce ICP-MS Octopole Reaction System, operating in standard (no collision cell gas) mode for Cerium (Ce). The instrument is UKAS accredited and was set up following standard operating procedure (SOP) INS/A1-0013. The samples were defrosted and equilibrated to room temperature, then shaken, to ensure homogeneity. An aliquot of 0.2g – 0.23g was taken from each sample and digested in a CEM Discover microwave, SOP INS/A1-0014, using a mixture of HNO_3/H_2O_2. The digested samples were then diluted to 5g prior to analysis. The samples were digested and analysed over a period of 5 days. Validation was carried out following SOP INS/A1-0015, this includes spiked recoveries and replicate analyses.

3.2.2 Results

The limit of detection (LoD) and limit of quantitation (LoD) are given in Table 8. The estimated uncertainty at 95% confidence (k = 2) is 20% for Ce. Results below the LoQ are likely to have a higher uncertainty.

Table 8. Limit of detection (LoD) and Limit of quantification (LoQ) for Ce.

	Ce concentration (ng g^{-1})
LoD	0.2
LoQ	0.8

The results for all CeO_2 NMs in ng/g as received are presented in Table 9.

Table 9. Data showing the ICP-MS test results for cerium concentration. The ICP-MS measurement was used to evaluate the concentration of CeO_2 NMs (extracted supernatant) over time when dispersed in one of four different media: a) DI water b) fish medium c) daphnia medium d) seawater. The last column gives the medium blank concentration of Ce.

Type of media	Day	Cerium concentration of the supernatant extracted (ng g^{-1})			Medium blank concentration of Ce (ng g^{-1})
		NM-211	NM-212	NM-213	
a) DI water	2	1.67	2.49	N/A	1.38
	6	1.83	2.9	1.88	
	9	2.06	1.94	1.05	
	14	1.87	5.08	1.79	
	21	2.7	1.59	1.33	
b) Fish	2	1	1.09	1.55	1.5
	6	1.75	1.72	2.61	
	9	2.37	2.22	3.96	
	14	1.9	1.57	1.42	
	21	3.1	1.58	1.35	
c) Daphnia	2	N/A	1.91	1.78	1.43
	6	1.68	2.02	1.93	
	9	N/A	1.7	1.43	
	14	1.62	1.68	1.92	
	21	22.4	1.64	3.45	
d) Seawater	2	1.22	1.92	2.01	1.57
	6	4.83	3.95	5.76	
	9	4.76	1.88	3.17	
	14	5.92	1.97	6.09	
	21	9.23	2.19	2.52	

Regarding the results shown in Table 9, there is no clear correlation between length of time and amount of CeO_2 in the supernatant for any of the CeO_2 NMs in any of the media, except for NM-211 in seawater. In general the amount of CeO_2 in the supernatant remains at the same level throughout this testing, though fluctuating a little. Comparing NM-211 and NM-212 to NM-213 (i.e. comparing the nanoforms to the macroform) does not indicate significant differences in amount of CeO_2 in the supernatant between forms.

3.3 Water Solubility/Dialysis

3.3.1 Method

The dissolution of NM-211, NM-212 and NM-213 in synthetic softwater medium without EDTA and buffered at pH 6.5 ± 0.1 with 2 mM piperazine-N,N'-bis(ethanesulfonic acid) (PIPES: Sigma-Aldrich) (US EPA, 1994) was determined using the equilibrium dialysis technique (flask method) described by Rogers et al., (2010). Cole Parmer Spectra/Por 7 dialysis membranes with a molecular weight cut-off of 1000 Dalton (~1 nm nominal pore size) and 45 mm diameter were cut into 9 cm lengths with a Teflon-coated razor blade and washed thoroughly in Milli-Q water. The dialysis cells were filled with 10 mL Milli-Q water and sealed with acid washed (1% v/v HNO_3) plastic dialysis clips. A concentrated suspension of cerium oxide was prepared for each type of nanoparticle by accurately weighing 0.12 g CeO_2 into polycarbonate vials, pipetting 10 mL deionised water into the vial, and sonicating for 30 minutes. The suspension was then shaken vigorously and quantitatively transferred into 3 L of synthetic softwater to achieve 40 mg/L CeO_2 in solution. Triplicate tanks were utilised in dialysis tests so that three replicates were sampled at each time-point. The dialysis cells were added to the test solution and continually stirred under constant light and temperature (24 °C) conditions for 72 hours. The total volume of the dialysis cells was kept to below 5% of the test solution in order to minimise dilution effects as dissolved cerium diffused into the dialysis cells. A cell was removed from each triplicate tank at each sampling time and an aliquot of solution was removed from the cells by pipette. A 5 mL volume of the external solution was also withdrawn using a syringe and filtered through a 0.1 µm filter (Pall) at each time point to measure the cerium in this fraction. Total cerium was measured at the start and end of the experiment. The samples were acidified to 0.5% v/v HNO_3 (Merck tracepur) and the cerium concentration measured by ICP-MS (Agilent 7500ce).

3.3.2 Results

The solubility of NM-211, NM-212 and NM-213 based on the flask dialysis method is presented in Table 10.

Table 10. Solubility of NM-211, NM-212 and NM-213.

Material	Dispersion medium	pH	Solubility
NM-211	EPA medium	6.5	< 1 µg/L
NM-212	EPA medium	6.5	< 1 µg/L
NM-213	EPA medium	6.5	130 µg/L*

*72 h solubility as there was no plateau in the concentration over time

As seen from the data NM-211 and NM-212 are at best only slightly soluble, as is NM-213. However, when comparing among the CeO_2 materials the bulk NM-213 is much more soluble than the nanomaterials NM-211 and NM-212.

3.4 Crystalline phase

3.4.1 Method

Crystallite phase was determined by using a Bruker ASX-D8 X-Ray Diffractometer using Cu Kα radiation over a 2θ range of 5^o to 85^o with a step size of 0.02^o.

3.4.2 Results

The XRD scans for NM-211, NM-212 and NM-213 are shown in Figure 11 together with the standard for CeO_2. The only detectable crystallite phase in NM-211, NM-212 and NM-213 was cubic cerionite.

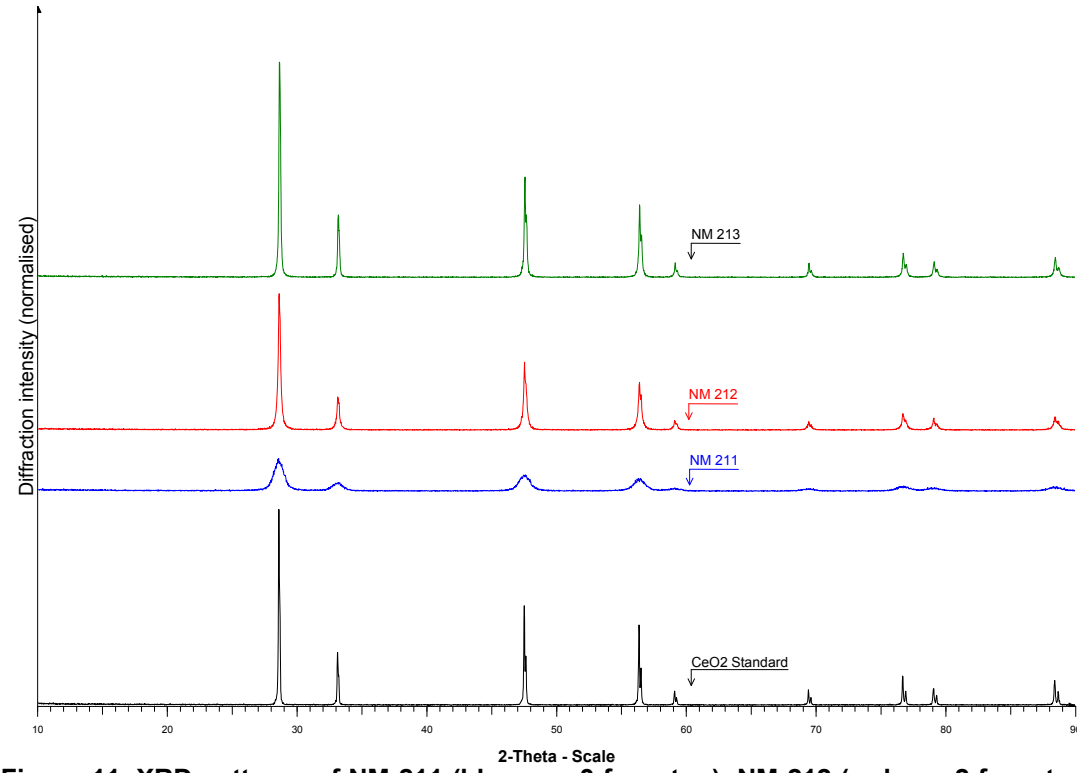

Figure 11. XRD patterns of NM-211 (blue, no. 3 from top), NM-212 (red, no. 2 from top) and NM-213 (green, top), together with the CeO_2 cubic cerionite structure reference lines (bottom).

3.5 Dustiness

3.5.1 Method

The dustiness of the materials was investigated using the rotating drum method specified in the European standard of the dustiness of bulk samples (EN15051). This device uses two porous size-selective foam stages and a filter to provide information about the dustiness of the powders in terms of the inhalable, thoracic and respirable fractions (WHO) of the dust dispersed. Three replicate tests of the powder were performed to obtain an estimate of the precision of the measurements. EN15051 also requires sample moisture content measurements to be made for each material as dustiness has been found to depend on moisture content. Analysis was carried out at 50 + 5% relative humidity (RH). NM-213 was also tested as received for its propensity to generate dust in standardized agitation.

The method used for these measurements is a downscaled version of the EN15051 rotating drum dustiness test (Schneider and Jensen, 2008). In summary, the dustiness index is conducted by measuring the total filter-collected mass release of respirable and inhalable dust (in mg/kg powder) during 33 repeated agitations for 1 minute and 2 minutes subsequent collection of the airborne residual dust. The collection efficiency of the inhalable dust fraction practically follows the efficiency curve for inhalability in calm air and hence underestimates the index as compared to conventional inhalability. On-line monitoring of particle size distributions are made by a Fast Mobility Particle Size (FMPS) Model 3091 (5.6 to 560 nm) and an Aerodynamic Particle Sizer (APS) Model 3022 (0.7 to 20 µm) (both from TSI Inc.). APS size data for particles smaller than 0.7 µm were not used due to poor counting efficiency.

Six grams of NM-213 material was tested in each quantitative run in a 50% RH HEPA-filtered test atmosphere at ambient temperature. Each material was tested in triplicate after an initial saturation run, which prevents underestimation of emission potential by wall- and tube loss. The average flow through the 5.9 L drum was 11 L/min. The mass of collected dust was determined in a conditioned weighing room (20°C; 50% RH) using a Sartorius microbalance.

Particle size distributions are plotted using unit density, which strongly deviates from the true density of cerium dioxide. The density effect will be most pronounced for aerodynamic sizes.

3.5.2 Results

Table 11, Table 12, and Table 13 below present results of the dustiness testing. Table 11 gives the dustiness as fractions of inhalable, thoracic and respirable dusts. Table 12 presents the calculated coefficient of variation (COV) values of the results in Table 11. COV is the ratio of the standard deviation (SD) to the mean and is a measure of variability in relation to the mean. It is used to compare the relative dispersion in one type of data with the relative dispersion in another type of data. The data to be compared may be in the same units, in different units, with the same mean value, or with different mean values (Measures of Dispersion – Coefficient of Variation" - http://jimwright.org/WebEd/u02/we020304.htm)

Table 11. Mean and SD of the dustiness results as inhalable, thoracic and respirable fractions of dust dispersed and moisture content of NM-211, NM-212 and NM-213.

Material	**Inhalable fraction** (mg kg^{-1})		**Thoracic fraction** (mg kg^{-1})		**Respirable fraction** (mg kg^{-1})		**Moisture content** (%)	
	Mean	**SD**	**Mean**	**SD**	**Mean**	**SD**	**Mean**	**SD**
NM-211	2222	202	800	11	86	15	1.1	0.10
NM-212	2845	244	668	59	66	26	0.4	0.10
NM-213	278	9	80	9	22	10	0.2	0.05

Table 12. The calculated coefficient of variation (COV) values of the results in Table 11.

Material	**Inhalable fraction** (mg kg^{-1})	**Thoracic fraction** (mg kg^{-1})	**Respirable fraction** (mg kg^{-1})	**Moisture content** (%)
	COV (%)	**COV** (%)	**COV** (%)	**COV** (%)
NM-211	9.1	1.4	16.9	10
NM-212	8.6	8.8	39.6	23
NM-213	3.2	10.9	43.7	23

Table 13. The dustiness classifications of the NMs, ranging from Very Low to High.

Material	**Dustiness Classification**		
	Inhalable	**Thoracic**	**Respirable**
NM-211	Moderate	Moderate	Moderate
NM-212	Moderate	Moderate	Moderate
NM-213	Low	Low	Low

3.5.2.1 Gravimetric dustiness for NM-213

Test results showed very low respirable and inhalable dustiness levels of NM-213 powder, see Table 14. The respirable dustiness index, however, had a relatively large standard deviation.

Table 14. Dustiness indices for NM-213. *Due to an unusual filter-behaviour the dustiness index is based on only two test runs.

	Respirable (mg kg^{-1})	**σ**	**Inhalable** (mg kg^{-1})	**σ**
NM-213	12.6	11.7	172.2	54.1

The inhalable dustiness index is classified to be at the very low end of dustiness, see Figure 12. Not surprisingly, it is among the lowest dustiness levels so far observed for (nano)particulate powders, as NM-213 is bulk CeO_2 included for comparison. It is at the level below granulated zirconia tested by Schneider and Jensen (2008). Also the level of respirable dust was also very low, where the limit between "Very Low" and "Low" dustiness is 10 mg/kg.

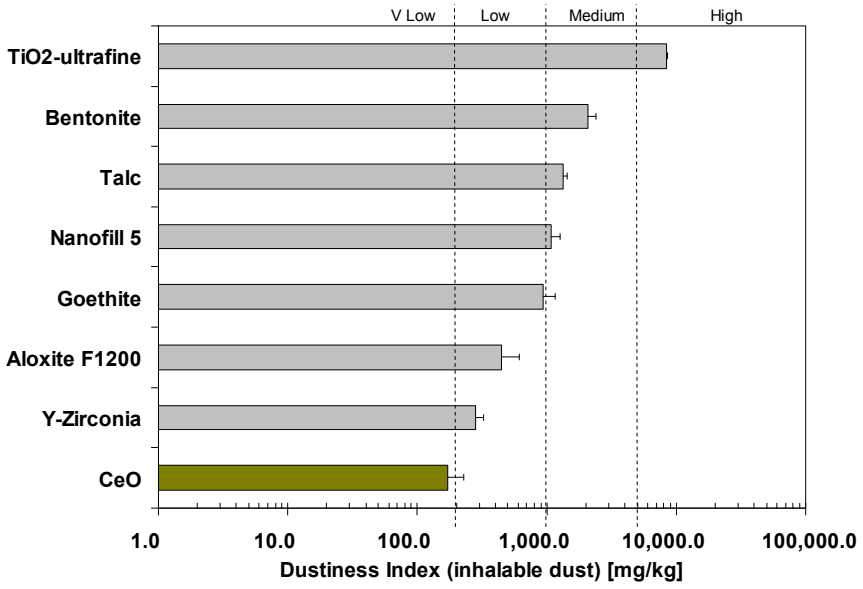

Figure 12. Inhalable dustiness index for NM-213 (bulk CeO_2) compared to data for other common powder materials. (Schneider *et al*. 2008; Jensen *et al.* 2009).

3.5.2.2 Size-distribution data for NM-213

Figure 13 shows the size distribution spectra of NM-213 measured by APS. The dust cloud consists of a relatively high number of small-size particles with a peak-mode around 30-40 nm and another major broad size mode ca. 200 nm. The dust in the µm-range appears to consist of two broad merged size-modes with a peak around 0.9 µm and between 3 and 4 µm, respectively.

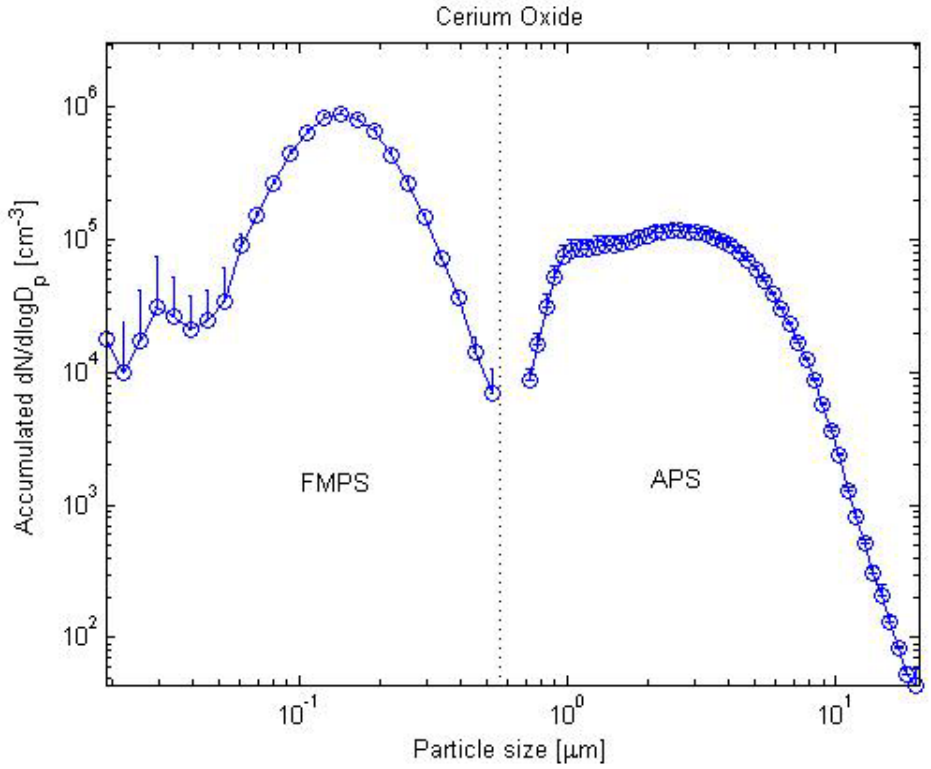

Figure 13. Particle number-concentration size spectra of NM-213. The dip in particle number concentration in the APS data below 1 µm is probably caused by a rapid drop in counting efficiency for sub-µm powders.

3.6 Crystallite size

3.6.1 XRD method, PROSPEcT

X-ray diffraction traces were obtained using a Siemens D5000 diffractometer. This consisted of a theta-theta goniometer and an NPL specimen stage. The X-ray source used for these measurements was the Cu- Kα X-ray (40 kV, 30 mA) filtered using a Ni filter that removed the Cu- Kβ component of the X-ray. The X-ray optics consisted of a 0.6mm anti scatter slit, a 1mm collimation slit and a 1mm detector slit. The diffraction measurement was conducted using coupled theta-theta drives in standard Bragg-Brentano geometry. The data was collected over a 2-theta range of 5 to 150° using a step size of 0.010° and a count time of 1.5 s/step. The diffracted data was electronically collected and stored on the laboratory PC. Prior to the measurement the X-ray beam was aligned by placing the X-ray source and the detector in line and passing the X-ray beam through a glass slit, the direct beam was attenuated using copper foil placed in front of the detector. Having aligned the two drives and the stage height a standard reference material (corundum) was used to check the alignment over a range of 2-theta values. Having collected the full diffraction trace the Scherrer equation was used to evaluate the crystallite size.

3.6.2 XRD results, PROSPEcT

Table 15 shows that crystallite sizes for the powders were in the range of 10 nm to 33 nm according to the NPL measurements. NM-211 has the smallest crystallite size, of 10.3 nm.

Table 15. XRD crystallite sizes determined using Scherrer's equation.

Material	Crystallite Diameter from XRD (nm) (NPL)	Crystallite Diameter from XRD (nm) (JRC)
NM-211	10.3	9
NM-212	33.3	49
NM-213	33.3	-

It is interesting to compare results of the crystallite size as obtained by X-ray diffraction (XRD) to those of particle size as obtained by SEM imaging. Overall, results show that particle size (as reported from SEM image analysis) is much larger than the corresponding reported crystallite size. This is not surprising as a particle (or grain) may consist of several different crystallites.

3.6.3 XRD method and results, JRC

The JRC made an XRD investigation of NM-211 and NM-212, using a Bruker D8 Discover multipurpose X-ray diffractometer, set up with the sample always in a horizontal position (theta-theta goniometer). The instrument uses a Cu-K□ X-ray source (long fine focus) at 40 kV and 40 mA, and can be rapidly software-switched between two different diffraction geometries. In parallel beam mode it employs a Goebel mirror in the incident beam and 0.2° Soller slits in the diffracted beam, while in focussing (Bragg-Brentano) mode there are motorised slits in the primary and diffracted beams, as well as vertical divergence Soller slits. The detector is a 1-D position sensitive Lynxeye detector that can be switched between 1-D and 0-D modes. The instrumental resolution in parallel beam mode is slightly above 0.2°, while in focussing mode the resolution is high enough not to be of concern for the investigation of the sample here. Measurements on NM-211 and NM-212 were taken both in parallel beam mode at a fixed incident angle of 6.0° as well as in the higher resolution focussing mode in order to obtain reliable data for crystallite size determination. The diffracted data was electronically collected and stored on the instrument PC and a K□-2 stripping routine was applied before the Scherrer equation was used for crystallite size determination.

For NM-211, both the Bragg-Brentano (the higher resolution method) and glancing angle scans give a crystallite size of 9 nm. The agreement between the two measurements is due to the wide peaks, which makes the instrumental resolution not so important, and the value should be rather accurate.

For NM-212, the Bragg-Brentano determined crystallite size is about 49 nm, assuming the full peak width is due to crystallite size broadening. The real value is likely to be slightly higher due to the non-zero instrumental resolution. The glancing angle method gives a crystallite size of about 37 nm, calculated with an instrumental resolution of 0.2 degrees, while a change of instrumental resolution to 0.25 degrees gives a calculated crystallite size of 49 nm. This illustrates that for larger crystallite sizes the higher resolution method is needed to get accurate values since there is some error in the instrumental resolution for the parallel beam geometry and there are errors introduced by the deconvolution process where the instrumental broadening is in the order of, or higher than, the real peak broadening.

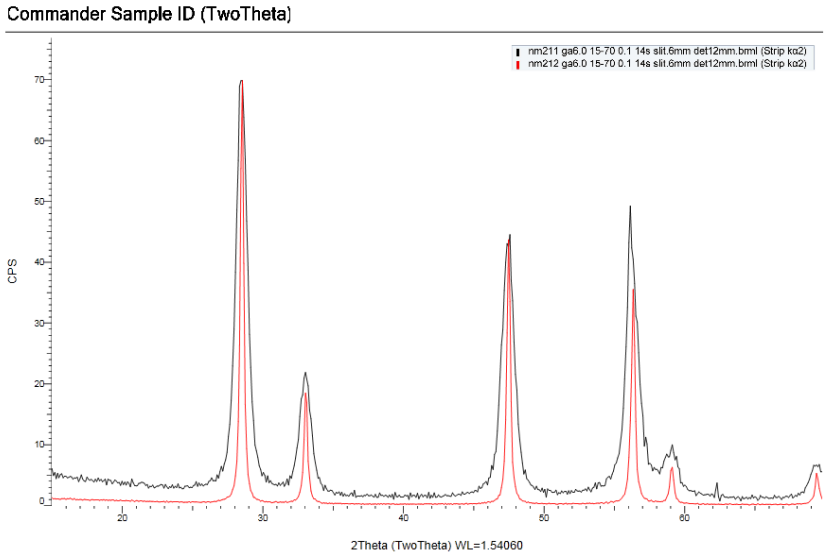

Figure 14. Parallel-beam scans (Kα-2 stripped) of NM-211 (black) and NM-212 (red), taken at an incident angle of 6.0°.

The peaks for NM-212 (red) are sharper than the peaks from NM-211(black) which indicate that the average NM-212 crystals are larger than the average NM-211 crystals. The TEM images confirm that NM-212 particles (TEM shown in Figure 17) are larger than NM-211 particles (TEM shown in Figure 15).

3.7 Representative TEM picture(s)

3.7.1 Method

Samples in Figure 15, Figure 17 and Figure 19 were prepared on carbon-coated grids (copper, 300 mesh) that had been glow discharged in nitrogen for 30 seconds to render them hydrophilic. Samples were dispersed by briefly sonicating a few mg of the material in approximately 20 µL ethanol to form a milky dispersion. 5µl of dispersion was applied to the freshly glow discharged grids. After 2 mins adsorption time, excess dispersion was wicked off using filter paper (Whatman 541) and the grids were air-dried for 15 minutes.

Grids were examined using a Tecnai 12 TEM (FEI, Eindhoven, Netherlands) operating at 120 kV, and micrographs were recorded using an Olympus Megaview III CCD camera (Tokyo, Japan) running AnalySiS imaging software (Olympus) at a variety of magnifications chosen to highlight both the aggregation state of the samples (lower magnifications e.g. 6 000x) as well as higher magnifications adequate for showing particle morphology (100 000x - 360 000x)

Samples in Figure 16, Figure 18 and Figure 20 were prepared on ultra-thin carbon film deposited on lacy carbon coated copper grids (copper, 300 mesh). The samples were dispersed by making a 200 mgL^{-1} suspension of material in water that was ultrasonicated with a high-power probe for 20 s (18 mm probe, 2 s pulsed duty cycle). A 6 µL drop of the resultant suspension was then placed on the shiny side of the grid and allowed to dry in a clean nitrogen atmosphere overnight. These grids were then examined using a CM120 Biofilter TEM (Philips, Eindhoven, Netherlands) operating at 120 kV. These grids were imaged at a magnification of 71 000x.

3.7.2 Results

3.7.2.1 Results for NM-211

Figure 15 and Figure 16 are TEM images of NM-211. Qualitative TEM analysis indicates that primary NM-211 particles appeared to be near spherical rather than polyhedral with regular morphology and a relatively homogenous size distribution. Generally, primary NM-211 particles have an aspect ratio close to 1 and with sizes between < 10 - 20 nm.

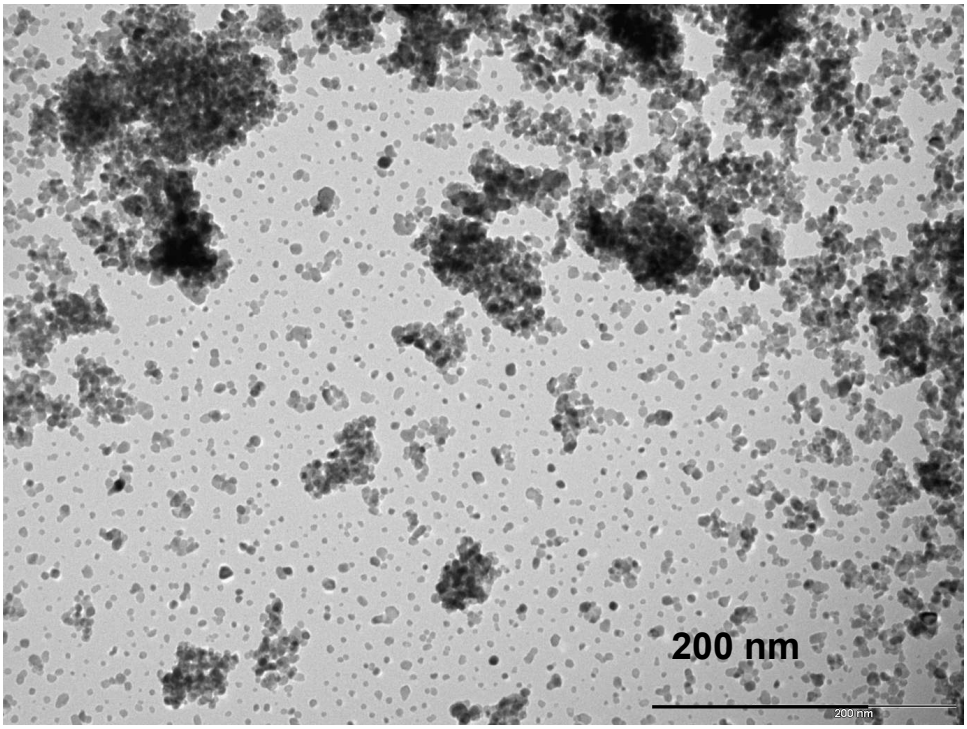

Figure 15. TEM image of NM-211, showing a regular primary particle size with presence of aggregated/agglomerated structures.

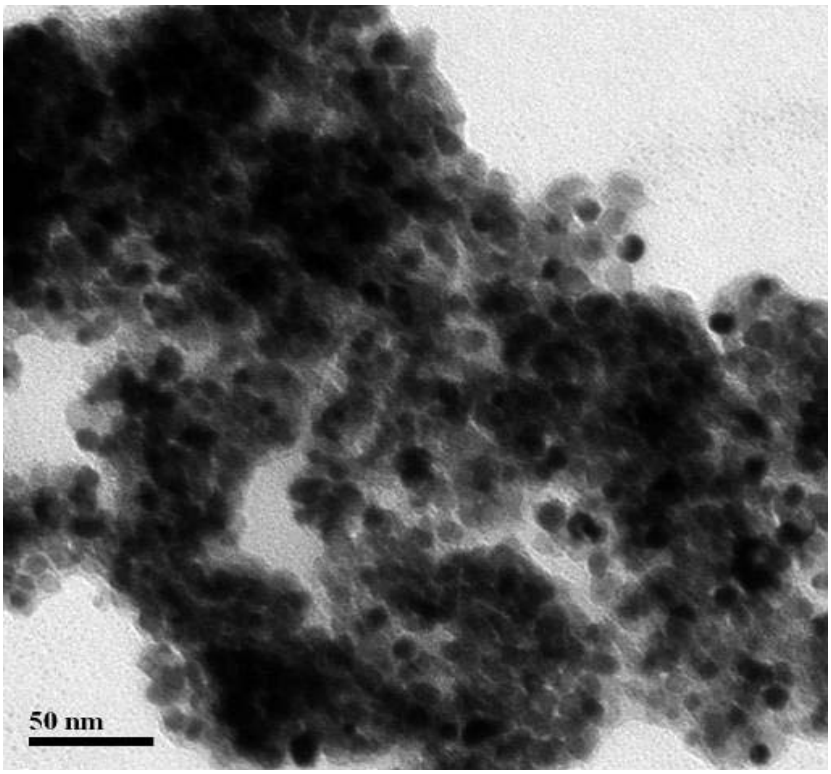

Figure 16. TEM image of NM-211, showing a regular primary particle size variation in an aggregated/agglomerated structure.

3.7.2.2 Results for NM-212

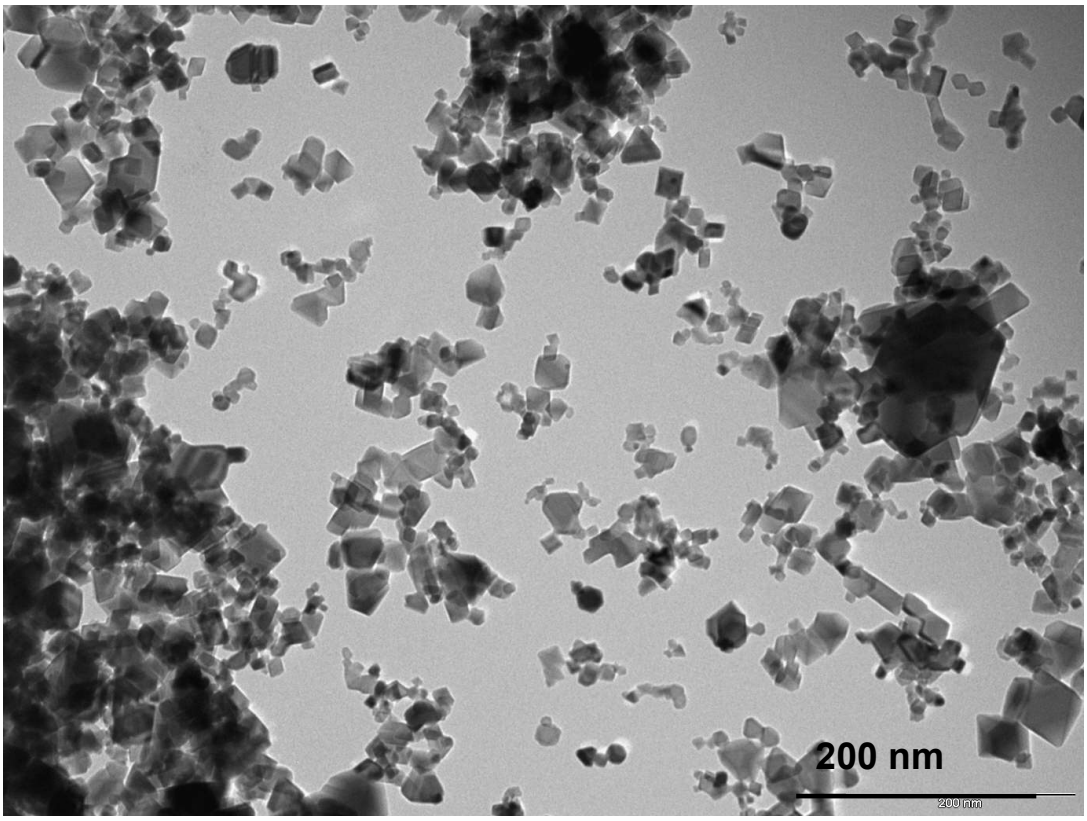

Figure 17. TEM image of NM-212, showing irregular and non-homogeneous primary particle size variation.

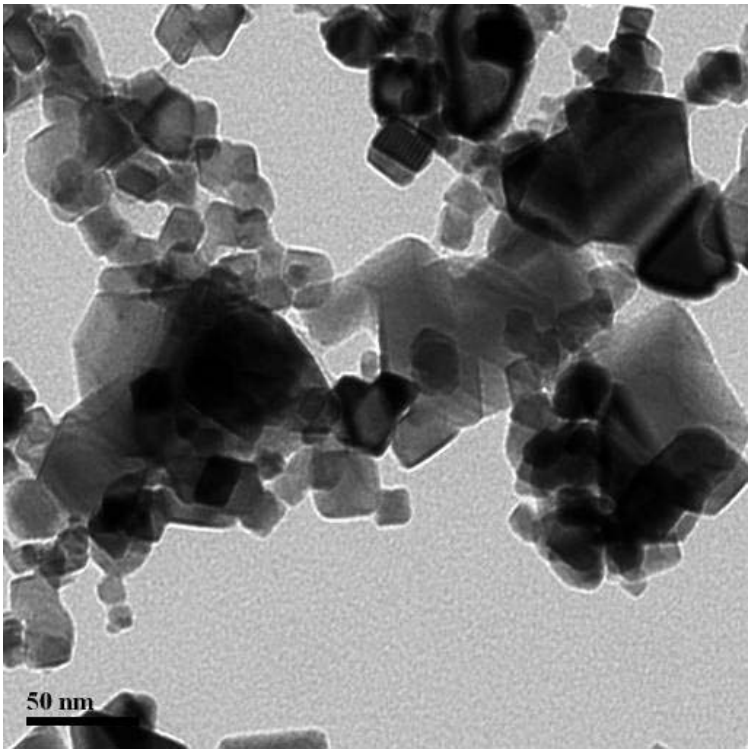

Figure 18. TEM image of NM-212, showing irregular and non-homogeneous primary particle size variation.

Figure 17 and Figure 18 are TEM images of NM-212. Qualitative TEM analysis indicates that primary NM-212 particles appeared to be polyhedral with irregular morphology and a non-homogenous size distribution, ranging from below 10 nm to well in excess of 100 nm. The primary NM-212 particles show a slight increase in aspect ratio with increasing particle size.

3.7.2.3 Results for NM-213

Figure 19 and Figure 20 are TEM images of NM-213. Qualitative TEM analysis of NM-213 indicates large polyhedral particles (150-200 nm) with irregular morphology that have associated with them a distribution of small sized particles (< 50 nm).

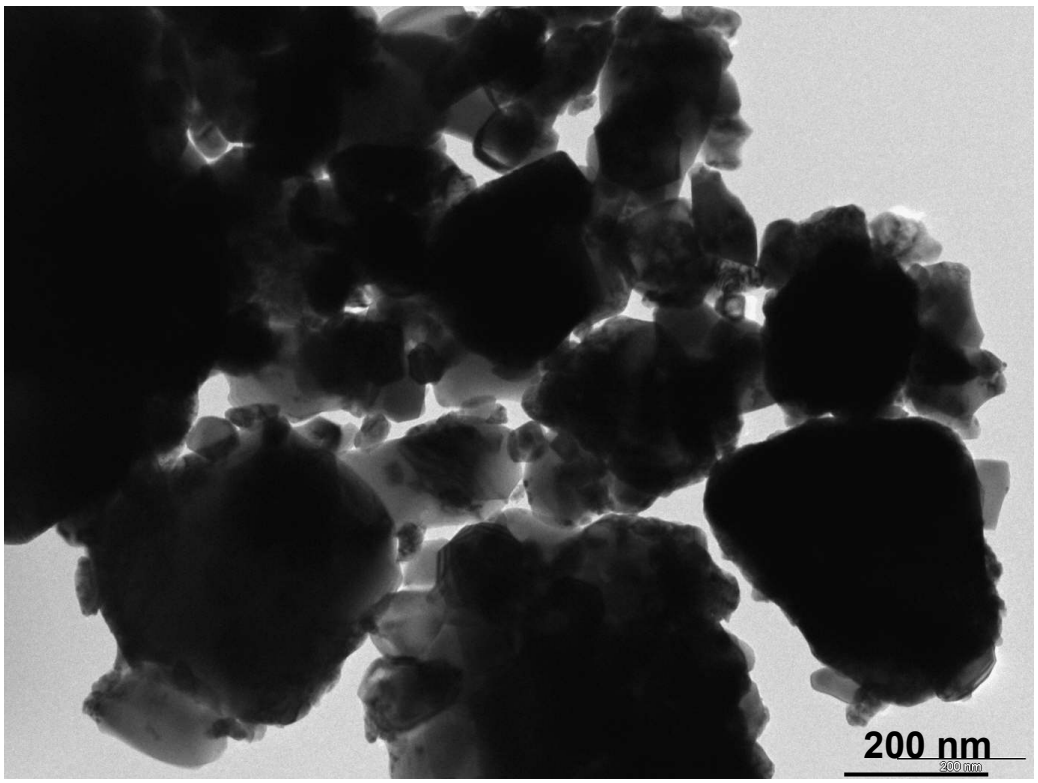

Figure 19. TEM image of NM-213, showing a relatively heterogenous distribution of larger particles with associated smaller particles.

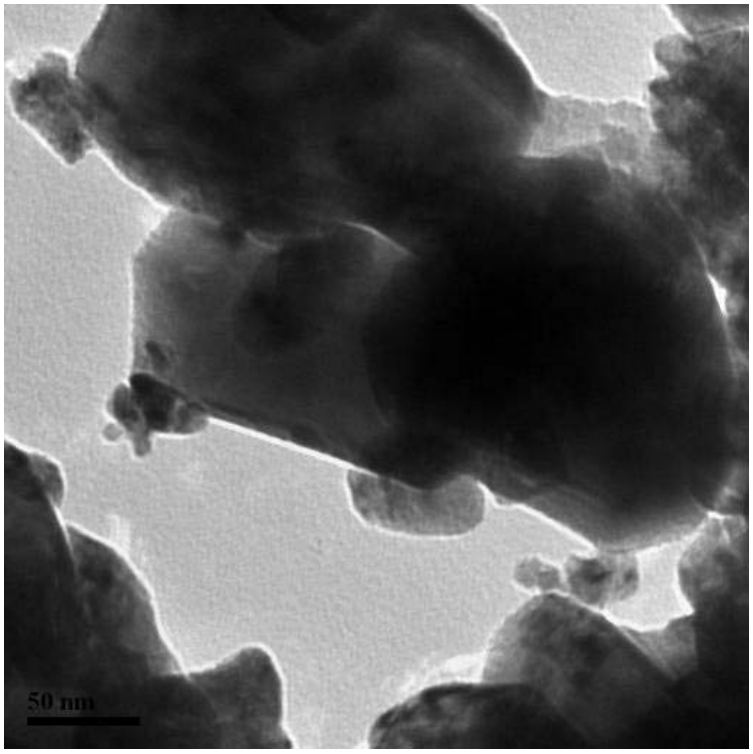

Figure 20. TEM image of NM-213, showing some small particles associated with a relatively homogeneous distribution of large particles.

TEM analysis indicates that all samples had a population of primary particles below 100 nm. NM-212 and NM-213 had polyhedral primary particles with variable sizes and morphology. NM-211 was the most size and shape-homogeneous with near spherical primary particles of size ~10-20 nm.

3.8 Particle size distribution

3.8.1 SEM Image Analysis

3.8.1.1 Method

SEM micrographs were analysed manually; this was done by manually tracing contours of primary particles on to a transparency sheet. The transparency sheet was scanned for further image analysis using ImageJ software, which automatically calculated particle diameter dimensions.

3.8.1.2 Results

Table 16 shows the corresponding mean Feret's diameter (of the primary particles) of NM-212 and NM-213; the analysis was not done for NM-211. Here, we report Feret's diameter, which is a parameter that is widely used in imaging of irregular shaped particles. Feret's diameter can be defined as the "maximum calliper length" i.e. the longest distance between any two points along the selection boundary (Chang *et al.* 2002). Overall, results show that particle size (as reported from SEM analysis) is much larger than the corresponding reported crystallite size by XRD. This is not surprising as a particle (or grain) may consist of several different crystallites.

Table 16. Size of primary particles, as defined by their corresponding Feret's diameter. Mean diameter (± 1 SD) of a minimum of 50 particles measured from the SEM images; the SD here represents the broadness of the size distribution (not error).

Material	Mean Feret's diameter/nm from SEM images
NM-212	28.4 ± 10.4
NM-213	615.3 ± 430.5

Table 16 also shows the SD associated with the mean particle size; the SD value will give an indication of polydispersity i.e. polydispersity will increase as SD becomes large.

3.9 Specific surface area

3.9.1 Method

BET surface area measurements were determined using Autosorb-1 (Quantachrome Instruments). The Autosorb-1 was calibrated using a quartz rod of a known volume, which is traceable to NIST. This calibration was then further checked using two BAM certified reference materials: BAM-PM-102 (nominal specific surface area (SSA) 5.41m^2g^{-1}) and BAM-PM-104 (nominal SSA 79.8 m^2g^{-1}). These two reference materials allowed the range of SSA of the nanoparticles to be encompassed with known specific surface area materials, thus adding confidence to the measurements. Surface area measurements were acquired using an 11-point BET gas adsorption method, with nitrogen as the adsorbate. Prior to analysis, the powdered sample was transferred to a sample bulb, then sealed and subsequently de-gassed overnight at 300°C under a high vacuum and subsequently weighed on an analytical balance in order to determine the sample mass after the degassing step.

3.9.2 Results

Table 17 summarises the results of BET specific surface area measurements. Results show a wide range of the specific surface area values for various NM powders i.e. from 4.3 to 66 m^2/g. Results show that NM-211 has the largest surface area (66 m^2/g) and the smallest being NM-213 (4.3 m^2/g). The variation in specific surface area of the CeO_2 NMs corresponds well with their inverse proportional variations in particle and crystallite sizes as shown in Table 17.

Table 17. Summary of the specific surface area values as obtained by the BET gas adsorption technique; the data is the mean of values (± 2 SD) of two replicates acquired on different days.

Material	Mean BET SSA (m^2/g)
NM-211	66 ± 2
NM-212	27.2 ± 0.9
NM-213	4.30 ± 0.10

BET specific surface area measurements were repeated using a Tristar II 3020 (Micromeritics) and an Autosorb iQ2 (Quantachrome Instruments). Surface area measurements on the Micromeritics 3020 were acquired using an 11-point BET gas adsorption method, with nitrogen as the adsorbate. Measurements on the Quantachrome iQ2 were acquired using a 5-point BET gas adsorption method, with nitrogen as the adsorbate. Prior to analysis, the powdered sample was transferred to a

sample bulb, then sealed and subsequently de-gassed overnight at 300 °C under a high vacuum and subsequently weighed on an analytical balance in order to determine the sample mass after the degassing step.

The mean BET specific surface areas of a different set of samples from the same batch to that reported above were determined using Micromeritics and Quantochrome instrumentation and are provided in Table 18.

Table 18. Summary of the specific surface area values as obtained by the BET gas adsorption technique; the data are the means of values (± 2SD; SD) collected from two different instruments.

Material	Mean BET SSA (m^2/g)
NM-211	64.9 ± 4.1
NM-212	27.8 ± 1.5
NM-213	4.8 ± 1.3

The surface area data sets were in good agreement between the two laboratories showing little variation and consistent with TEM data on particle size.

3.10 Zeta potential (surface charge)

3.10.1 Method

Electrophoretic measurements were obtained using a Zetasizer Nano ZS (Malvern Instruments, UK) equipped with a 633 nm laser. The reference standard (DTS1230, zeta-potential standard from Malvern) was used to qualify the performance of the instrument. Sample preparation involved filling of a disposable capillary cell (DTS1060, Malvern). Prior to their use, these cells were thoroughly cleaned with ethanol and de-ionised water, as recommended by the instrument vendor. For analysis, the individual cell was filled with the appropriate sample and flushed before re-filling; measurement was carried out on the second filling Malvern Instrument's Dispersion Technology software (Version 4.0) was used for data analysis and zeta-potential values were estimated from the measured electrophoretic mobility data using the Smoluchowski equation.

3.10.2 Results

The measured zeta-potential values for the NMs (50 mg/L) are summarised in Table 19.

Table 19. The mean values of zeta-potential (of six replicates) for different nanomaterials dispersed in various media at a concentration of 50 mg/L. Values are the mean and ± 1 SD of six replicates.

Material	DI water (mV)	DI water + 5mM NaCl* (mV)	Fish medium (mV)	Seawater (mV)	Daphnia medium (mV)
NM-211	28 ± 2	23.0 ± 1.3	-15.3 ± 0.6	N/A	-17.4 ± 0.3
NM-212	33 ± 2	33.9 ± 1.7	-11.1 ± 1.0	N/A	1.2 ± 0.2
NM-213	-7 ± 6	-2 ± 2	-22.3 ± 0.5	N/A	-15.0 ± 0.3

* DI water + 5 mM NaCl - this medium was employed to compare with the DI results when in the presence of inert background electrolyte

Results show that zeta-potential values of NMs when dispersed in seawater cannot be successfully measured (due to high conductivity) and thus displayed as N/A on the table; such unsuccessful measurements were reported in the corresponding "quality report" at the end of the measurement. In general, results indicate high zeta-potential values for NMs that are dispersed either in DI water (or DI water + 5 mM NaCl), and thus confer stability in such media. This is true apart from NM-213 where dispersion in DI resulted in the least stable dispersion. Furthermore, results also show that apart from NM-213, values of zeta-potential measured were lower when the NMs were dispersed in an ecotoxicology media indicating much poorer dispersion stability in such media. Overall, NM-213 has the opposite behaviour i.e. least stable in DI water (and DI water + NaCl)

and most stable in fish and daphnia media. Currently, no explanation is available for this behaviour.

An apparent charge reversal for NM-211 and NM-212 is observed, in going from DI water to fish medium. Particles dispersed in DI water exhibit a net positive charge, whereas particles in fish medium generally exhibit a net negative charge, suggesting that one or more of the components in the fish medium are adsorbed on CeO_2 particles causing this effect. This charge reversal is also apparent when NM-211 is dispersed in daphnia medium.

3.11 Surface chemistry

3.11.1 Method, PROSPEcT

XPS spectra are obtained by irradiating a material with a beam of X-rays while simultaneously measuring the kinetic energy and number of electrons that escape from the top 1 to 10 nm of the material being analysed. It requires ultra-high vacuum (UHV) conditions.

XPS measurements were obtained in ultra-high vacuum using a Kratos AXIS Ultra DLD (Kratos Analytical, UK) instrument fitted with a monochromated Al Kα source, which was operated at 15kV and 5mA emission. Photoelectrons from the top few nanometres of the surface were detected in the normal emission direction over an analysis area of approximately 700 x 300 micrometres. Spectra in the range 1400 to –10 eV binding energy and a step size of 1 eV, using a pass energy of 160 eV were acquired from selected areas of each sample. The peak areas were measured after removal of a Tougaard background. The manufacturer's intensity calibration and commonly employed sensitivity factors were used to determine the concentration of the elements present. High-resolution narrow scans of some of the peaks of interest were acquired with a step size of 0.1 eV and 20 eV pass energy. (The manufacturer calibrated the intensity calibration over the energy range). The energy scale was calibrated according to ISO 15472 Surface chemical analysis – X-ray photoelectron spectrometers – Calibration of energy scales. However, the charge neutraliser was used when acquiring the spectra, which shifted the peaks by several eV. The C 1s hydrocarbon peak (285 eV binding energy) was used to determine the shift for identifying the peaks.

Samples were prepared using carbon adhesive tape to affix them to 1 cm copper squares. Care was taken to cover the tape with the powders as completely as possible but some samples had better coverage than others and in many cases a signal was detected from the tape as well as the powder itself. The tape contained oxygen and silicon in addition to carbon.

3.11.2 Results, PROSPEcT

The elemental composition of the different NM powders as measured by XPS (i.e. at the surface: 0 to 12 nm depth) is summarised in Table 20, in which the elemental concentrations of the elements: carbon (C), cerium (Ce) and oxygen (O) are shown. As evident from the results, there was a significant contribution of carbon and this can be largely attributed to surface contamination on the particles. Areas of best coverage were selected for analysis and XPS analysis of the carbon tape itself showed a composition of

74% C, 21% O and 5% Si. From the lack of any significant signal from Si on samples, it was estimated that there was better than 90% coverage within these analysis areas. A different sample preparation procedure could be adopted to separate background carbon signal from that on the particles during XPS measurements.

Table 20. XPS element atomic concentrations results; the powders were spread on to an adhesive carbon tape.

Material	C 1s (%)	Ce 3d (%)	O 1s (%)
NM-211	36.3	20.2	43.5
NM-212	75.2	2.0	22.9
NM-213	66.7	5.6	27.7

Table 21 shows a preliminary attempt to determine the oxidation states of cerium dioxide NMs from three different suppliers. The values were obtained using a "ten peak fit" method (Zhang *et al*, 2004). In summary, this method involved peak fitting the relevant narrow scan spectra and subsequently attributing peaks to Ce^{4+} or Ce^{3+} valence states.

Table 21. XPS results, PROSPEcT of the cerium-based oxide Nanomaterials and the proportion of Ce^{4+}: Ce^{3+} in the mixture.

Material	Ce^{4+} $[CeO_2]$ (%)	Ce^{3+} $[Ce_2O_3]$ (%)
NM-211	94.3	5.7
NM-212	93.1	6.9
NM-213	92.0	8.0

The XPS results indicate that all cerium-based oxide nanomaterials consist of a mixture of Ce^{4+} and Ce^{3+} species; NM-212, NM-213 and NM-211 dry have similar ratios of Ce^{4+}/Ce^{3+}. This is a different result from the JRC measurements where no presence of Ce^{3+} was observed, see Figure 23.

In a second set of experiments, samples were filled into individual wells of a powder sample holder (1 well per sample) and analysed as received. Samples were then analysed using a Kratos HS spectrometer under standard conditions, the sampling depth being several nm (approx. 10 nm maximum) and the analysis area approx. 0.3 mm × 0.7 mm. Samples were analysed at 2 different times approximately 2 months apart. Table 22 presents the average of these two data sets.

Table 22. Chemical surface composition of all NMs: atomic concentrations (%).

	NM-211	NM-212	NM-213
Ce	26.13 ± 1.87	25.73 ± 0.44	22.17 ± 0.07
Zn			0.92 ± 0.1
O	42.92 ± 0.32	42.14 ± 0.43	39.21 ± 1.58
C	30.94 ± 2.2	31.87 ± 0.93	37.3 ± 1.42

In all NM-21x cerium, carbon and oxygen were detected. It is unclear what the specific form of carbon is but it is thought to be due to surface contamination or adsorbed carbon containing species rather than a bulk component. Only for NM-213, the presence of Zn was indicated. This observation is consistent with data obtained from ICP-AES where NM-213 had significantly higher levels of detectable Zn. All NMs showed good elemental stability over the sampling time period with consistent levels of Ce, O and C being detected.

3.11.3 Method, JRC

The JRC performed XPS analysis of NM-211 and NM-212. The experimental procedure and equipment were as follows: NM-211 and NM-212 were compressed into pellets and mounted on the sample holder with double-sided ultra-high vacuum (UHV) compatible Cu tape. XPS measurements were performed with an AXIS ULTRA Spectrometer (KRATOS Analytical, UK). Instrument calibration was performed using a clean, pure Au/Cu sample and pure Ag sample (99.99 %). Measured values for electron binding energies (BE) were 84.00 ± 0.02 eV, and 932.00 ± 0.05 eV. The samples were irradiated with monochromatic AlKα X-rays (hν = 1486.6 eV) using AN X-ray spot size of 400 x 700 μm^2 and a take-off angle (TOA) of 90° with respect to the sample surface. The base pressure of the instrument was lower than $1x10^{-8}$ Torr and the operating pressure lower than $3x10^{-8}$ Torr. A filament (I = 1.9 A) was used to compensate for surface charging and all spectra were corrected by setting hydrocarbon 285.00 eV.

For each sample, a survey spectrum (0-1110 eV), from which the surface chemical compositions (at%) were determined, was recorded at pass energy of 160 eV. In addition, one set of high-resolution spectra (PE = 20 eV) was also recorded on each sample. The analysis time was kept below 20 minutes to avoid any X-ray damage to the sample (Rama et al., 1997).

The data were processed using the Vision2 software (Kratos, UK) and CasaXPS v16R1 (Casa Software, UK). Sample compositions were obtained from the survey spectra after

linear background subtraction and using the RSF (Relative Sensitivity Factors) included in the software derived from Scofield cross-sections. This method is estimate to give an accuracy of 10% in the measurement of elemental compositions. Curve fitting of C1s peaks was carried out using the same initial parameters and inter-peak constraints to reduce scattering. The C1s envelope was fitted with Gaussian-Lorentian function (G/L=30) and variable full width half maximum.

3.11.4 Results, JRC

The surface compositions of NM-211 and NM-212 are reported in Table 23 and in Figure 21 (a) and (b), examples of survey spectra of the two NMs are shown.

As can be seen from Table 23 the surface of the sample is strongly contaminated with Carbon (C), which is thought to come from hydrocarbons in the ambient air; the XPS measurements indicate that the carbon is bound as H-C-H, C=O, O-C=O and HO-C=O. In particular, the hydrocarbon contamination is higher in the pellet samples indicating that the pressing procedure is a possible source of further surface contamination respect to the as received materials.

Table 23. Surface compositions obtained from the survey spectra recorded on the pellet and the powder pressed samples. (Standard deviation in brackets)

Material	C at%	O at%	Ce at%
NM-211 pellet	28.1 (0.5)	60.4 (0.7)	11.4 (0.4)
NM-212 pellet	28.6 (3.0)	59.4 (2.2)	11.7 (1.0)
NM-211 pellet Ar etched	4.2 (0.1)	64.3 (0.9)	29.9 (1.5)
NM-212 pellet Ar etched	6.1 (1.0)	64.0 (0.5)	31.5 (1.0)
NM-211 pressed	20.5 (1.7)	65.0 (1.2)	14.5 (1.1)
NM-212 pressed	19.5 (1.7)	66.9 (1.2)	13.6 (0.9)
NM-211 pressed Overnight in UHV	22.3 (2.5)	62.2 (1.6)	15.6 (1.3)
NM-212 pressed Overnight in UHV	21 (2.5)	64.4 (2.7)	14.6 (0.4)

The ratio of Ce to O is about 0.18 for the pellets and about 0.25 for the pressed samples, which is quite far from the theoretical 0.5, indicating a strong adsorption of oxygen on the surface of the nanoparticles; it should be noted that calculation of composition with such of high level of contamination is not precise. As this result was not expected, a second set of samples from new (i.e. previously unopened) vials was

measured, resulting in similar outcome. Moreover, because it has been suggested that permanence in UHV could cause variation in the composition of cerium oxides (Zhang et al., 2004), an additional analysis of the powder pressed samples after a 24 h period in the analysis chamber ($p \sim 10^{-8}$ Torr) was performed, and the results are presented in Table 16. As can be seen, the composition of the samples does not change much after the permanence in UHV environment. The Ce/O ratio is 0.24 and 0.22 for NM-211 and NM-212, respectively, definitely comparable with the values obtained after 1 h in UHV. Moreover, the shape and intensity of the Ce 3d and 4d spectra (not shown) did not change indicating that the UHV is not affecting the initial oxidation state of Ce.

Since the pellet samples show higher contamination, analysis after Ar ion etching (3keV, I=1.5uA, $p=1x10^{-7}$ Torr) was also performed. The compositions after etching are reported in Table 23. As can be seen the carbon contamination decreases and, as expected, the Ce and the O signals increase. The Ce/O ratio is now 0.46 and 0.48 for NM-211 and NM-212, respectively. These values are definitely closer to the cerium oxide theoretical stoichiometry of 0.5.

However, analysis of the O1s peaks, see Figure 22, before and after ion etching indicate that although the hydrocarbon contamination is strongly reduced, the presence of OH and C-O moieties onto the surface of the nanoparticles is still detected (components at about 531.5eV). Moreover, the component at 529.5eV, which corresponds to the cerium oxide is also decreasing; this indicates a chemical reduction of ceria by the ion bombardment in agreement with published papers (e.g. Qiu et al., 2006). This is also supported by the analysis of the Ce3d core level spectra as discussed below.

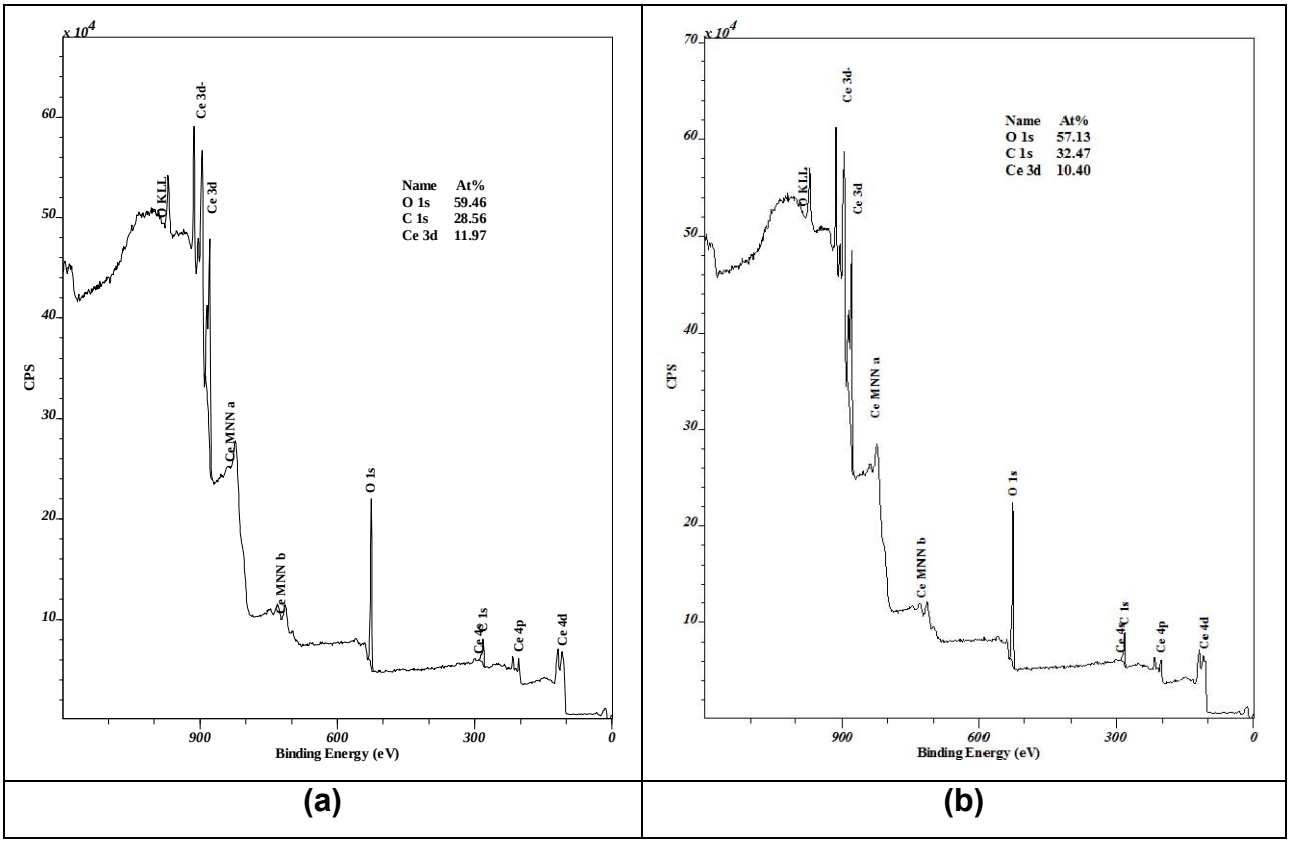

Figure 21. Survey spectra of (a) NM-211 and (b) NM-212.

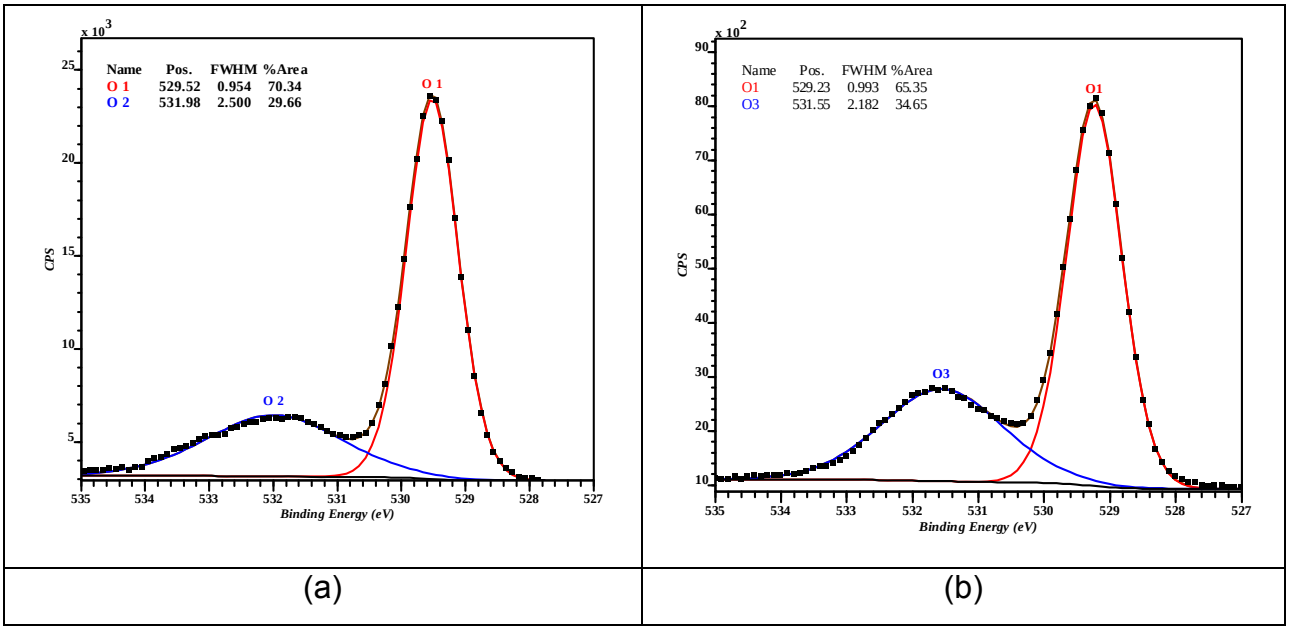

Figure 22. O1s core level spectra of NM-212 powder pressed sample: (a) before Ar ion etching and (b) after 5 min etching at 3keV Ar^+.

In Figure 23, the Ce 3d core level spectra of NM-211 and NM-212 are reported.

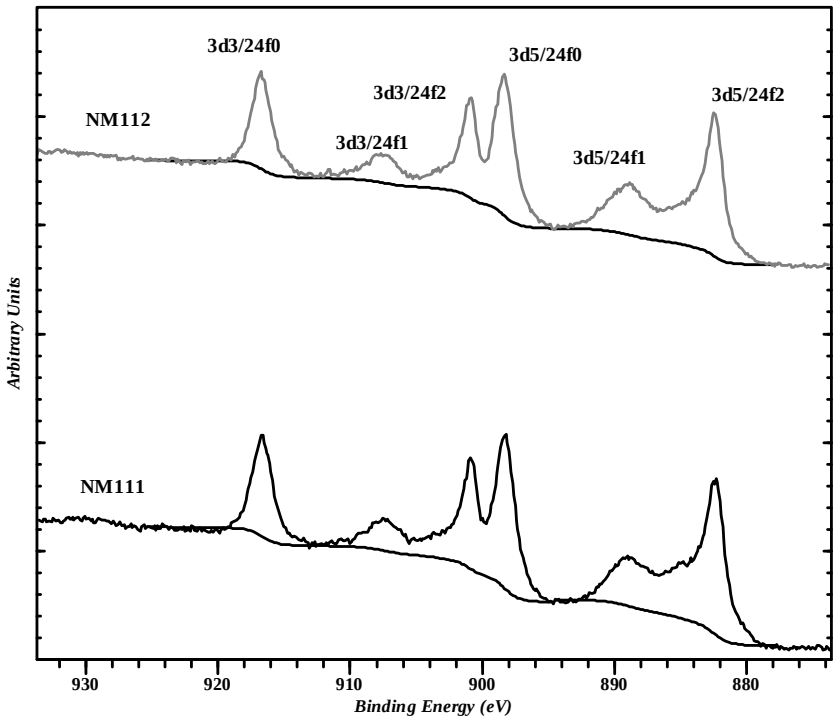

Figure 23. Ce3d core level spectra of NM-211 (bottom) and NM-212 (top).

There are several studies of cerium oxide using XPS and many conclusions have been drawn from these results (e.g. Holgado et al., 2000; Paparazzo et al., 1991; Hendersen et al., 2003). However, the analysis of the Ce 3d high resolution spectrum is not straightforward.

As a first attempt of deducing some information on the Ce oxidation states, we have assigned the different peaks of the Ce3d spectrum following the work published by D. Baer and co-workers (Baer et al., 2013) and using this as a basis the spectra for both NM-211 and NM-212 indicate that cerium is present mainly in oxidation state 4+. No evident signs of Ce^{3+} are observed.

The possible presence of Ce^{3+} can be investigated by fitting the Ce 3d envelope with different components, as presented above in section 3.11.1. However, this fitting is complicated by the presence of “shake-up” and “shake-down” satellites (Ratutoiu, N. and Teodorescu, C.M., 2013). The shake-up satellites are additional lines appearing at higher binding energies (lower kinetic energies) respect to the parent line (Koopman line). These satellites correspond to photoelectrons that lose energy by excitation of a resonance in the sample (e.g. plasmon losses). On the other hand, the shake-down satellites, appearing at lower binding energies (higher kinetic energies) with respect to

the parent Koopman line, are due to the switch from a state specific of a localized orbital to one corresponding to a delocalized orbital. The shake-down satellites are quite frequent in atoms with 4f electrons. In the case of Ce3d, as can be seen from Figure 23, both Ce3d levels ($Ce3d_{5/2}$ and $Ce3d_{3/2}$) have associated satellites.

Given these complicated physical effects, the fitting of the Ce3d core level spectra was found to be quite difficult. Moreover, different models have been proposed to take into account the multiple physical phenomena related to cerium oxide photo-emission.

These complications with the fitting are believed to be a major reason why the XPS measurements performed by the different institutions gave different results regarding the presence of Ce^{3+}.

In summary, XPS analysis gives information on the surface composition of the investigated material. The results for NM-211, NM-212 and NM-213 indicated that their surfaces are composed mainly of oxygen, O^{2-}, and cerium, which may be present as Ce^{4+} and Ce^{3+}; Ce^{4+} is the predominant oxidation state. In addition, for NM-213 also the presence of zinc was identified. As briefly outlined in this section, the identification of Ce^{3+} is complicated and dependent on models selected for data fitting, and thus the presence Ce^{3+} was suggested by one of the two laboratories performing analysis. The catalytic properties of cerium are based on its changes in oxidation state. Furthermore, the surfaces of NM-211, NM-212 and NM-213 are contaminated with carbon that is thought to come from hydrocarbons in ambient air. As the surface of the particles is the site at which reactions are believed to take place the surface composition is an important element of the particles' possible reactivity.

3.12 Porosity

3.12.1 Method

Porosity may be determined using the Brunauer-Emmett-Teller (BET) and Barrett-Joyner-Halenda (BJH) method of analysis of adsorption and desorption isotherms to determine pore area, specific pore volume and pore size distribution independent of external area due to the particle size of the sample. The t-plot method is commonly used to determine the external surface area, pore volume and pore surface area in microporous solids.

3.12.2 Results

Table 24 presents the micropore surface area and volume, external surface area and a determination of the average pore width for all four samples.

Table 24. Summary of the specific surface area values as obtained by the BET and BJH gas adsorption technique.

Material	t-Plot Micropore Surface Area: m^2/g	t-Plot External Surface Area: m^2/g	t-Plot micropore volume: cm^3/g	BJH Desorption average pore width (4V/A): Å
NM-211	3.8623	58.0885	0.001511	102.019
NM-212	0	27.0668	0	121.736
NM-213	0.5117	3.3671	0.000223	184.302

All NMs have very low or no microporosity. The major contribution to total surface area is from external surfaces and is thus predominantly determined by particle size and shape rather than high internal porosity. NM-211 has the highest surface area and micropore volume of all the NMs consistent with particle size observations.

3.13 Redox potential

3.13.1 Method

Redox potential was measured using an ORP Oakton® Waterproof ORP Testr®, purchased from Cole Palmer UK; this measures the potential difference across two electrodes i.e. a Pt (platin) electrode against a double junction Ag/AgCl reference electrode. The electrode was used in accordance to the manufacturer's instructions. Prior to use, the electrode was pre-conditioned in tap water for 30 minutes before rinsing in distilled water. When making the measurements, the electrode was carefully placed in a vial containing the sample; there must be sufficient liquid sample to cover the sensing element. The electrode was carefully stirred a little and then placed in a fixed position, slightly above the bottom of the container. The signal output was allowed to settle for 5 minutes before a reading i.e. the "field potential" was noted. After measurement, the electrode was cleaned with tap water and rinsed with distilled water, after which further measurements can be made. When not in use, the electrode was stored in a solution of Oakton® electrode storage solution, as recommended by the manufacturer.

The redox potential ORP electrode was calibrated against YSI® Zobell ORP Calibration Solution (purchased from Cole Palmer); this reagent was made available in dry form and was reconstituted with 125 mL of DI water prior to use, after which the solution has ~ 6 months expiry date. This standard solution was also used to verify the performance of the electrode in the beginning and at the end of the study.

For Ag/AgCl reference, the redox potential value for Zobell solution was 231 ±10 mV (depending on temperature); at ~ 20 °C, this value was ~ 237 mV. Redox potential measurements were carried out on freshly dispersed NM in various media: DI water and the three ecotoxicology media (fish, daphnia and seawater).

All field potential values recorded were subjected to an additive correction factor of +206 mV; this was necessary for the final value to be reported as if the reference electrode was a standard hydrogen reference electrode instead of the Ag/AgCl.

Dispersion of each nanomaterial in the appropriate liquid media was carried out in accordance to the protocol recommended in PROSPEcT, see section 4.2.

3.13.2 Results

Table 25 below gives an overview of the results, and includes information on the medium blank measurements.

Table 25. Redox potential of NM dispersion in various liquid media, the value quoted is relative to the standard hydrogen reference electrode; values quoted in mV; the ORP probe electrode is used. The last two columns report the redox potential of liquid media blanks only and associated pH values.

Medium	CeO_2			Media Blanks	
	NM-211	NM-212	NM-213	Medium Blank	pH
DI water	414	416	422	405	N/A
Fish media	436	439	430	418	7.34
Daphnia media	426	415	429	425	7.94
Seawater	387	384	382	384	8.75

There is still some ambiguity concerning the redox potential parameter i.e. as to what and how to measure, particularly when in a nano-ecotoxicological context. The study investigates the redox potential measurements, using ORP probe electrode, of various CeO_2 dispersions, in various liquid media. Although the redox potential values acquired from ORP electrode may be indicative of the redox state of the entire system, it is difficult to quantify the reliability of such measurements.

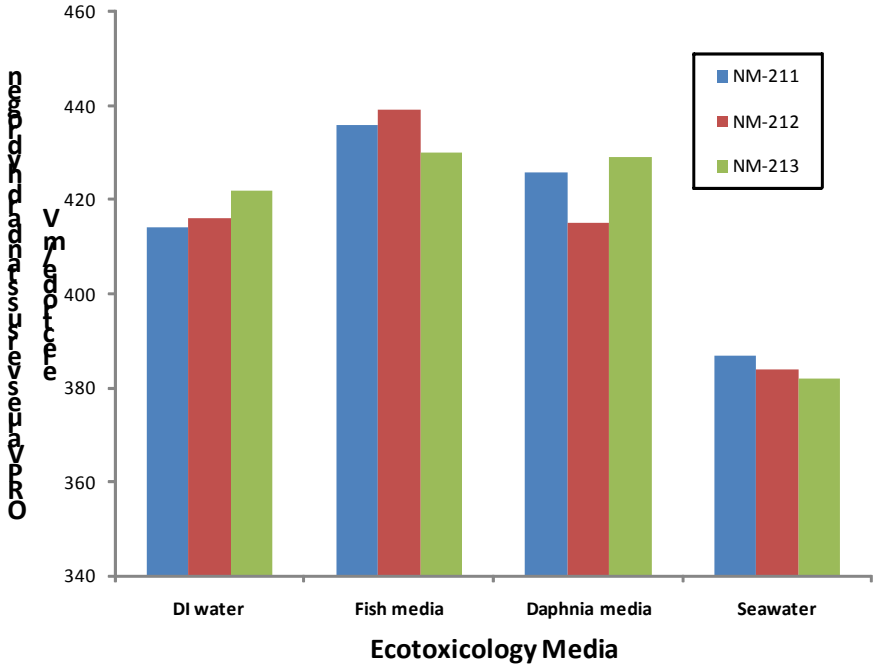

Figure 24. Graphs of results summarized in Table 25. (Redox potential of NM dispersion in DI water, fish media, daphnia media and seawater, in mV).

3.14 Photocatalytic Radical Formation Potential

3.14.1 Method

A 5 M KI (Sigma, St. Louis, MO, USA) solution in ultra-pure water was freshly prepared; shaking and vortexing was preferred to sonication to dissolve KI. KI solution was added to the samples of NMs as received after dispersion (50mg/L), to obtain a typically 1 mL volume sample, with 0.1M KI. 6 x 3 samples were prepared for each NM/media combination. Additionally, 6 x 3 samples containing 0.1 M KI only and 50mg/L anatase NMs (Anatase Nanopowder, Sigma) for each media were prepared as negative and positive controls respectively; 6 NM samples plus controls were prepared and assessed in total. All samples were contained in individual 2mL microcentrifuge tubes. Samples were irradiated under a 1kW Solar Simulator (Newport Corporation, Stratford, CT). The instrument possesses a Personal wavelength correction^{TM} Certificate by Newport. The irradiance of the Solar Simulator was measured to be 1000 Wm^{-2} using an optical power/energy meter (Newport, model 842-PE). Irradiation was performed on groups of 40 microcentrifuge tubes. The tubes were placed vertically under the centre of the lamp of the solar simulator, on an in-house made polystyrene holder, their cups having been removed. The samples were subjected to 10 min periods of irradiation, followed by 5 min period of non-irradiation to reduce sample overheating. After each 10 min period, 1x3 samples for each NM/media combination and controls were removed from the irradiations. Samples irradiated for 0 min, 10 min, 20 min, 30 min, 40 min and 60 min were collected for each NM/media combination and controls. The samples containing NMs were centrifuged at 20800 rcf (relative centrifugal force) for 15 min and 800 μL of supernatant was collected in a new micro-centrifuge tube and then analysed using UV-visible spectroscopy.

The UV-visible spectrum (absorbance scans from 300 nm to 500 nm) was acquired for samples that were irradiated for 60 minutes. Optical absorbance at 352 nm was acquired for all samples. Absorption spectra were acquired with a Lambda 850 UV-Vis spectrometer supported by UV Winlab software [Version 5.1.5] (Perkin Elmer, Waltham, MA). The instrument wavelength calibration was checked using Holmium glass standards (Serial # 9393, Starna Scientific, Hainault, UK). For the reference channel of the spectrophotometer a matched cell containing the corresponding dispersing media (with no nanoparticles) was used. Absorption spectra were acquired on samples that have been irradiated for 60 minutes. Absorbance scans from 300 nm to 500 nm were performed, using a slit width of 2 nm and a scan rate of 50 nm/min. After each sample, the cuvette was cleaned with a 2% solution of Hellmanex detergent, rinsed with pure

water and ethanol and then blow-dried. Optical absorbance at 352nm was performed using a plate-reader Victor^3 1420 multilabel counter (Perkin Elmer), supported by Wallac 1420 software (Perkin Elmer). 300μL of each sample (supernatant after centrifugation) was placed in the wells of a 96-well plate. Only the wells of rows 2 to 6 and columns 1 to 10 were used, as they had the same level of noise. The absorption at 352nm was measured using a 0.1s measurement time. Measured absorption values were displayed on a 0 arbitrary unit (a.u.) to 2 a.u. scale.

3.14.2 Results

Figure 25 shows the UV-visible spectra of tri-iodide ions, as produced when TiO_2 anatase nanopowder particles (positive control) are dispersed in four different media, in the presence of KI. The dispersions were exposed for 60 minutes, under 1000 W/m^2 white light irradiation. Results show that the spectra exhibit typical maxima at 352 nm, see Figure 25. The absorbance values at 352 nm can be used to quantify tri-iodide concentrations (ε = 26000 Lmol^{-1}cm^{-1}).

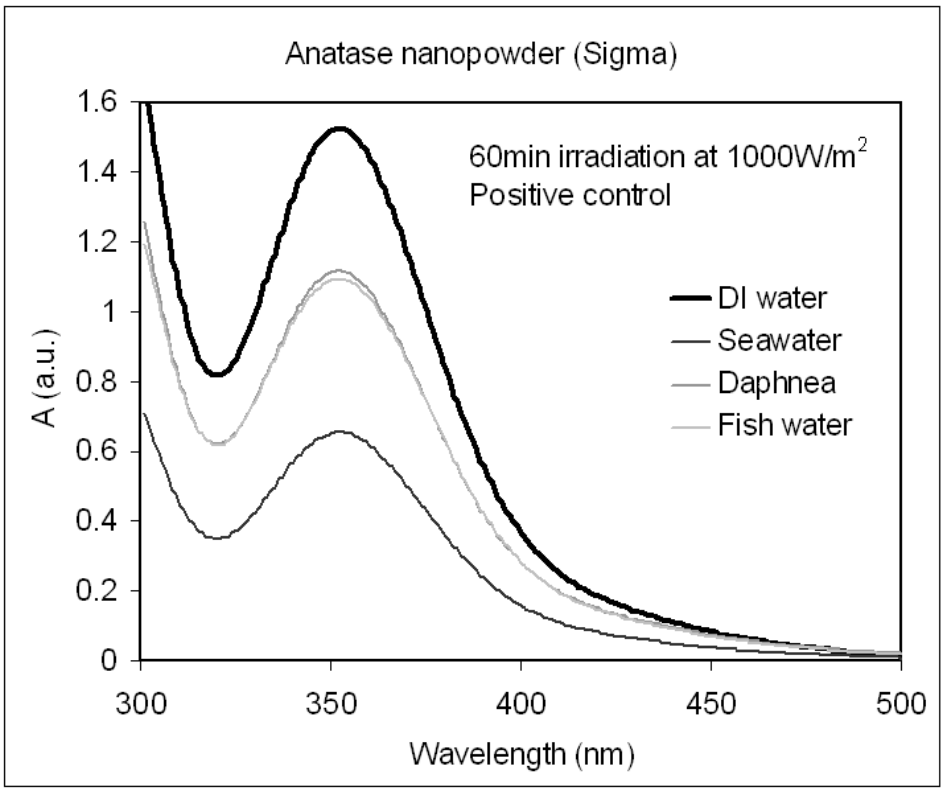

Figure 25. UV-Visible absorption spectra of anatase NM (TiO_2) (positive control) in 4 different media (DI water, seawater, daphnia and fish media) after being irradiated with solar simulator at 1000 W/m^2, for 60 minutes.

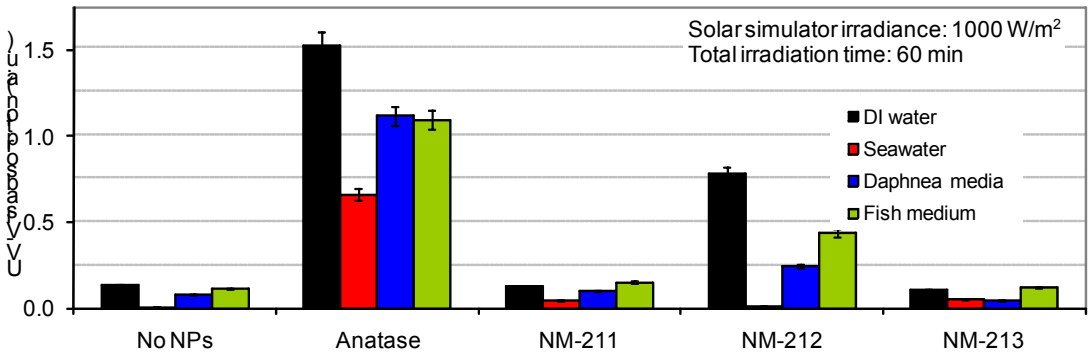

Figure 26. Absorbance readings at 352 nm, of NM-21x in 4 different media (DI water, seawater, daphnia and fish media) after being irradiated with solar simulator at 1000 W/m^2, for 60 minutes. Anatase NM (TiO_2) dispersed in the four different media was used as positive control; media with no NMs were used as a negative control. The values are normalized to the absorption measured for the negative control in DI water.

Figure 26 compares the absorption measured at 352 nm for the NM-21x samples in 4 different media after 60 min of total irradiation; the corresponding negative control (i.e. media with no NMs) are also shown. Results show that there was a certain level of tri-iodide (I_3^-) measured in the irradiated sample containing media only. Interestingly, tri-iodide was suppressed in seawater and this may be attributed to a higher concentration of ions (potentially with some scavenging capacity either to ROS species or to electron (or holes) at the NM surface) in this media. As expected, results for TiO_2 anatase, being the most active photocatalytic material, show a much higher rate of tri-iodide formation than the CeO_2 NMs. In particular, the absorbance signal was highest in DI water, with the lack of ionic species in the media. Again, when in seawater, the absorbance signal was reduced (similar to the corresponding blank (seawater)). There are several possible explanations for this:

1. Presence of scavengers in solution, as previously described.
2. Enhanced aggregation/sedimentation of the NMs in seawater media compared to other media.

NM-212 has a trend similar to TiO_2 anatase, in having the largest absorbance signal in DI water and the smallest when in seawater. For NM-211 and NM-213 the absorbance signals were within a range similar to that of the irradiated blank. Samples that were kept in the dark exhibited no absorption peak at 352 nm.

Lastly, a UV-visible plate reader was used to follow the cumulative production of I_3^- with varying irradiation time; this was quantified by measuring absorption at 352 nm. In summary, results show (figure not included here) that absorbance signal generally

increases with irradiation time and this can be attributed to the increase in the amount of ROS being generated. Again, the results are consistent with previous observations, in that:

1. TiO_2 anatase gave the highest absorbance reading.
2. NM-212 had a trend similar to TiO_2 anatase i.e. largest absorbance reading in DI water and lowest when in seawater.

3.15 Other relevant information

3.15.1 Chemical Analysis

3.15.2 Method

All samples were prepared in duplicates using about 0.15 g for analysis. CeO_2 samples were dissolved using 1:1 HNO_3: H_2O_2 mixture on a hot plate for 30 minutes. Resultant solutions were diluted to 100 mL, internal standard Sc was added and the resultant solutions were analysed by Varian 730 Axial Inductively Coupled Plasma-Atomic Emission Spectroscopy (ICP-AES). Certified multi-element solutions were also used to check the accuracy of the method.

3.15.3 Results

Table 26 shows the outcomes of the elemental analysis.

Table 26. Outcome of the elemental analysis of NM-211, NM-212 and NM-213. All results are expressed in units of weight percentage and ppm. The spectral wavelength (in nm) for each element is indicated in the element column.

Element (spectral wavelength)	**Material**		
	NM-211	**NM-212**	**NM-213**
Ce* (446.021)	**83.09 %**	**81.62 %**	**84.05 %**
Al (396.152)	0.20%	0.20%	0.22%
Ca (422.673)	100 ppm	23 ppm	58 ppm
Co (238.892)	<2.5 ppm	<2.5 ppm	<2.5 ppm
Cr (267.716)	13 ppm	14 ppm	<1.5 ppm
Cu (324.754)	20 ppm	10 ppm	15 ppm
Fe (259.940)	<5 ppm	<5 ppm	<5 ppm
K (769.897)	<15 ppm	<15 ppm	<15 ppm
Mg (285.213)	<2 ppm	<2 ppm	<2 ppm
Mn (257.610)	6.0 ppm	5.8 ppm	6.0 ppm
Na (589.592)	64 ppm	20 ppm	45 ppm
Ni (231.604)	<20 ppm	<20 ppm	<20 ppm
P (213.618)	<90 ppm	<90 ppm	<90 ppm
Pb (283.305)	<40 ppm	<40 ppm	<40 ppm
S (181.972)	<200 ppm	<200 ppm	<200 ppm
Si (251.611)	35 ppm	20 ppm	16 ppm
Sn (283.998)	96 ppm	100 ppm	105 ppm
Ti (336.122)	8 ppm	6.2 ppm	6.6 ppm
V (311.070)	<0.02 ppm	<0.02 ppm	<0.02 ppm
Zn (213.857)	23 ppm	80 ppm	305 ppm
Zr (339.198)	25 ppm	25 ppm	26 ppm

* Theoretical Ce weight percentage in CeO_2 is 81.4 %.

In general all samples were found to have few or no secondary elements present. NM-211 and NM-212 had slightly higher levels of detectable alkali metals (Ca, Na) than NM-213. NM-212 and NM-213 appeared to have higher levels of detectable Zn than NM-211.

4 NM characterisation: As prepared test item in vehicle/media

This section describes the characteristics of the NM materials for nano-CeO_2 for the NM as prepared test items (see Section 2.3: Characterisation of the NM-Series). The measured results of the selected properties (characteristics) depend on the choice of vehicle or media and the conditioning protocol, and applied standard operating procedures. The term “vehicle” is used in Good Laboratory Practice (GLP) and generally used in studies regarding effects on human health. The term “media” is widely used in studies regarding environmental toxicology and fate. “Vehicle” and “media” thereby both describe the matrix, in which the test material is presented to the test system. The endpoints for hazard and fate are described in the Guidance Manual for sponsors. For typical in vitro tests, SOPs for test item preparation are presented together with the corresponding properties for materials investigated, here NM-211, NM-212 and NM-213. Stability of the dispersion should be addressed.

NM as prepared Test Item[3]

Dispersion in air/ aqueous media; physico-chemical properties:

(1) Size and size distribution, shape

(2) Agglomeration/ aggregation

(3) Zeta-Potential (aqueous media)

(4) Dispersibility, solubility

(5) Composition, purity

[3] see Section 2.3: Characterisation of the NM-Series.

4.1 The PROSPEcT Dispersion Protocol for CeO_2

The method below is developed for the preparation of nanoparticles dispersion (in particular zinc oxide and cerium dioxide) in DI water (concentration of 15 mg/L) but can be adapted (to other concentrations and/or aqueous based liquid media). The dispersion protocol and associated training video are available[4]. The user is advised to view the video before using the dispersion protocol.

4.1.1 Materials

1) 1 large glass beaker (1 L)
2) Volumetric (glass) flask (1 L)
3) DI water (resistivity of ~ 18 Ohm)
4) Ultrasonic probe[5] (Cole-Parmer ® 130-Watt Ultrasonic Processors (50/60 Hz, VAC 220); product number EW-04714-51); the probe is a 6 mm (1/4") titanium and is tuned to resonate at 20 kHz, ±50 Hz)
5) Mini Lab Jack
6) Stainless steel spatula
7) Disposable pipette (preferably standard glass Pasteur pipette, 150 mm length)
8) Vial 2 (as detailed above) containing the nanomaterial (~15 mg)
9) Vial 3 (pre-cleaned, with no specific dimensions) to contain a suitable volume of DI water (or ecotoxicology media), such that you will end up with 1 mg/ml nanoparticle concentration in Vial 2

4.1.2 Method

Step 1: Add a few drops of DI water (or liquid media) taken from Vial 3, using a glass pipette to the nanoparticle powder in Vial 2, in order to create a thick paste. Do this whilst mixing using a pre-cleaned spatula and apply sufficient energy to remove visible aggregates in the paste. The purpose of this wetting step is to sufficiently substitute solid-air interface with solid-liquid interface, as recommended by guidelines in BS ISO 14887 (2000) ["Sample Preparation – dispersing procedures for powders in liquids"].

Step 2: Add the rest of DI water from Vial 3 into Vial 2 (containing the paste of nanoparticle powder) and gently mix using a clean spatula.

[4] The PROSPEcT dispersion protocols can be viewed using the following link, http://www.nanotechia.org/activities/prospect-ecotoxicology-test-protocols-representative-nanomaterials-support-oecd.

[5] Although exposure of the nanoparticles to a high intensity ultrasonic probe appears to be more effective than other de-agglomeration tools, its limitations have not been fully investigated. For example, probe tip disintegration/erosion over time can potentially contaminate samples. Probes can also have highly variable performance, particularly at the lower end of the market. In addition, the high shear forces provided by the ultrasonic probe can alter nanoparticle structure and also increase the temperature of the dispersion.

Step 3: Place Vial 2 on to a lab jack and insert the ultrasonic probe tip half way down the small vial. De-agglomerate using an ultrasonic probe for 20 s (at 90 % amplitude; this should give a temperature rise of ~5 °C in the dispersion). The operator should determine the acceptable temperature rise during sonication in the given time period. If longer sonication time is required then the operator must provide a better control of the temperature inside the vial. One option is to immerse Vial 2 in an ice bath during the sonication. During sonication, ensure that the tip is not touching the sides of the glass vial. In addition, do not place your hands near the de-agglomerating unit whilst it is operating.

Step 4: Once completed, transfer the nanoparticle suspension to the desired total volume (to make the "stock") and mix gently with a glass rod. Flush the small vial with further DI Water (or liquid media) and add this to the rest of the suspension. This "washing" step is important to ensure that all of the nanoparticles are transferred from the small vial to the larger beaker, such that dosage measurement (by mass) can be interpreted accurately. Gently stir with a glass rod. For greater accuracy, make up to the desired volume using appropriate volumetric flask/ pipette.

Step 5: The dispersion is now ready for analysis. For the nanoparticle analysis, this will involve the sample splitting of "the stock". From guidelines found in ISO 14488:2007 ["Particulate materials sampling and sample splitting for the determination of particulate properties"] sample splitting using a pipette is recommended as this method (relative to sample splitting using multiple capillary tubes) is simple to do and less prone to contamination. Prior to taking an aliquot out of the stock, agitate the stock dispersion; this can be achieved by gently mixing using a clean glass rod to ensure homogeneity of the sample.

4.2 Other Dispersion Protocols

4.2.1 Protocol with Serum, the ENPRA protocol

The following dispersion method has been developed for the ENPRA[6] project and can be applied to NM-211, NM-212 and NM-213 (ENPRA, 2010) when dispersion in serum is desired. The ENPRA protocol has been used to disperse nanoparticles of titanium dioxide (NM-101, NM-105) (TiO_2), silver (NM-300, NM-300K) and multi-walled carbon nanotubes (NM-400, NM-401, NM-402).

4.2.2 Protocol with Bovine Serum Albumin (BSA), the Nanogenotox protocol

In some cases, it may be more appropriate to disperse the NMs in BSA rather than Serum depending on the standard operating procedure for the chosen test method and the corresponding test item preparation protocol. The protocol that has been developed in the Nanogenotox project[7] can also be applied to cerium dioxide NMs. The details are found on the Nanogenotox web-site at http://www.nanogenotox.eu/files/PDF/web%20nanogenotox%20dispersion%20protocol.pdf

4.2.3 Protocol in Cell Culture Medium for *in vitro* Toxicity Testing

Dispersion protocols for dispersion of NM-21X in F-12K biological cell culture media containing 10% foetal bovine serum using a sonicating water bath and measurement of their toxicity using the A549 cell line and for *in vitro* toxicity testing in e.g. MTT, WST-1 or Neutral Red uptake assay (NR) are described in the report "NM-Series of Representative Manufactured Nanomaterials. Zinc Oxide NM-110, NM-111, NM-112, NM-113. Characterisation and Test Item Preparation" by Singh et al. (2011)

[6] The ENPRA project is a major current European project funded by the European Commission under Framework Programme 7 to develop and implement a novel integrated approach for engineered nanoparticle risk assessment. Further details on ENPRA can be obtained from the project website, http://www.enpra.eu.

[7] NanoGenoTox is a Joint Action collaboration project funded by the Executive Agency for Health and Consumers (EAHC) under the Public Health Programme of the European Commission and supported by the European Commission - JRC. Further details on the Nanogenotox project can be obtained from http://www.nanogenotox.eu

4.3 Dispersion Stability Testing

In accordance to BS ISO 14488, successful (liquid) sample splitting can only be conducted if a homogeneous dispersion has been achieved – otherwise this will result in a much higher sampling error. Prior to sample splitting, the operator should check that the dispersion is sufficiently stable during the time period required to perform sample splitting and subsequent characterisation of the nanoparticle dispersion. For example, if the nanoparticle dispersion is to be characterised by Dynamic Light Scattering (DLS), then a suitable aliquot should be pipetted out from stock and the mean particle size measurement acquired. Six replicates should be measured to ensure that the sample is sufficiently stable within a reasonable period of time.

If there is evidence of aggregation/sedimentation in the sample, then the dispersion is not sufficiently stable to allow subsampling to be carried out without incurring sub-sampling error. In addition to errors incurred from sub-sampling steps, stability testing of the dispersion is important for nanoparticle characterisation. For example, for DLS measurement, one of the pre-requisites is that the sample is stable with no signs of sedimentation, as DLS is applicable only to particles that remain fully suspended undergoing Brownian diffusional motion, throughout the measurement to obtain reliable and accurate results.

4.4 Dispersion Characterisation Tools

Whatever the characterisation tools chosen, operators must be aware of the limitations posed by the various techniques. It is beyond the scope of this report to give detailed description of limitations of various techniques and so it is left for the operator to ensure that the technique chosen is suitable for a given nanoparticle dispersion. For example, in the case of DLS, this tool is not suitable to resolve a broad particle size distribution, as larger particles can (and usually does) mask the signal of smaller nanoparticles. In order to resolve multi-modal particle distribution, techniques that have a separation mechanism element integrated in the analytical tool will be more suitable e.g. Flow Field Flow Fractionation.

5 Conclusions

The JRC launched the repository for representative nanomaterials in February 2011, hosting more than 20 different types (8 chemistries) of nanomaterials at the JRC site in Ispra (Italy).

The representative nanomaterials were introduced by the JRC to support the OECD Working Party on Manufactured Nanomaterials' programme "Safety Testing of a Set of Representative Manufactured Nanomaterials", established in 2007, as well as national and international research projects within and outside the EU.

The OECD WPMN recommended testing selected nanomaterials for a series of end-points in the OECD nanomaterials testing programme. The cerium dioxides NM-211 and NM-212 are among the key nanomaterials of the programme, and they are compared to NM-213, which is a macro-form (bulk) of cerium dioxide. This report presents information on characterisation and test item preparation.

Also outside the OECD WPMN, characterisation of nanomaterials and applicable methods are intensively studied to understand nanomaterials both in a regulatory and a scientific context. For example, the JRC published recently a report regarding "Requirements on measurements for the implementation of the European Commission definition of the term 'nanomaterial'' (see Linsinger et al. 2012) that also evaluates the limits and advantages of the existing methods for characterisation of nanomaterials, and the reader is referred to it for additional information on the applicability areas of the methods.

The characterisation of the CeO_2 NMs was performed within the PROSPEcT project, and also at JRC for some of the end-points.

The properties of NM-211, NM-212 and NM-213 studied and described in this report demonstrate the NM-Series' relevance for use in measurement and testing studies, for example for hazard identification and related to safety of nanomaterials. The NM-series materials serve the need as representative nanomaterial, and they may at a later stage be used as performance standard and reference matrix for harmonisation and standardisation, method development, optimisation and validation.

5.1 Characterisation

Many of the OECD endpoints on physico-chemical testing have been completed in this report. Chemical analysis was performed on the CeO_2 NMs and in general they were found to have little or no secondary elements present. NM-211 and NM-212 had slightly

higher levels of detectable alkali metals (Ca, Na) than NM-213. NM-212 and NM-213 appeared to have higher levels of detectable Zn than NM-211.

The XPS results, giving information on the surface chemistry, for NM-211, NM-212 and NM-213 indicated that their surfaces are composed mainly of oxygen, O^{2-}, and cerium, which may be present as Ce^{4+} and Ce^{3+}, with Ce^{4+} being the predominant oxidation state. As outlined in section 3.11, the identification of Ce^{3+} is complicated and dependent on models selected for data fitting, and thus the presence Ce^{3+} was not suggested by all the laboratories performing analysis. The catalytic properties of cerium are based on its changes in oxidation state. Furthermore, the surfaces of NM-211, NM-212 and NM-213 are contaminated with carbon that is thought to come from hydrocarbons in ambient air. As the surface is the assumed reaction site of the particles, the surface composition is an important element of the particles' possible reactivity. In addition, the XPS analysis indicated the presence of zinc for NM-213, which is consistent with data obtained from ICP-AES where NM-213 had significantly higher levels of detectable Zn (305 ppm compared to 23 ppm (NM-211) and 80 ppm (NM-212) respectively.

SEM analysis indicates that the cerium dioxide NMs are highly agglomerated and aggregated. Particle size distribution using SEM image analysis shows that the Feret's diameter is smallest for NM-212 and largest for NM-213.

The only detectable crystallite phase in NM-211, NM-212 and NM-213 was cubic cerionite. The crystallite sizes determined by XRD were in the range of 9 / 10.3 nm (NM-211) to 33.3 / 49 nm (NM-212) and 33.3nm (NM-213). The SEM particle size of NM-213 is much larger than the XRD crystallite size as the macro-sized particles of NM-213 are composed of several crystallites.

TEM analysis indicates that all NMs had a population of primary particles below 100 nm. NM-212 and NM-213 had polyhedral particles with variable sizes and morphology. NM-211 was the most size and shape-homogeneous with near spherical primary particles of size ~10-20 nm.

DLS indicates that NM-211, NM-212 and NM-213 are polydisperse particles. CLS disc centrifuge results of measurements in four media, DI water, fish medium, seawater and daphnia medium, indicate that NMs are largest in seawater and smallest in DI water indicating that larger agglomerates exist in ecotoxicology media.

Turbidity measurements show that overall CeO_2 NMs are most stable when dispersed in de-ionised (DI) water and least stable when dispersed in an ecotoxicology media. This finding was not consistent with the corresponding zeta-potential results, in which dispersion was more stable in fish medium (i.e. -22 mV) when compared to DI water (i.e.

–7 mV). This apparent discrepancy is explained by the fact that dispersion stability was measured by two different methods.

Results show that zeta-potential values of NMs when dispersed in seawater cannot be successfully measured (due to high conductivity) and thus displayed as not applicable (N/A). In general, results indicate high zeta-potential values for NMs that are dispersed either in DI water (or DI water + 5 mM NaCl), and thus confer stability in such media. Results show values of zeta-potential measured were lower for NM-212 and NM-213 when dispersed in an ecotoxicology media indicating much poorer dispersion stability in such media. Overall, NM-213 has the opposite behaviour i.e. least stable in DI water (and DI water + NaCl) and most stable in fish and daphnia media. Currently, no explanation is available for this behaviour. Of interest is the apparent charge reversal for NM-212 and NM-211 observed, in going from DI water to fish medium. Particles dispersed in DI water exhibit a net positive charge, whereas particles in fish medium generally exhibit a net negative charge, suggesting that one or more of the components in the fish medium are adsorbed on CeO_2 particles causing this effect. This charge reversal is also apparent when NM-211 is dispersed in daphnia medium.

Specific surface area measurements using BET show a wide range of the specific surface area values for various NM powders i.e. from 4.3 to 66 m^2/g. Results show that NM-211 has the largest surface area of 66 m^2/g and the smallest being NM-213 of 4.3 m^2/g. The variation in specific surface area of the cerium dioxide NMs corresponds well with their inverse proportional variations in particle and crystallite sizes. BET measurements were repeated and the data sets were in good agreement between the two laboratories showing little variation and consistent with TEM data on particle size.

The CeO_2 NMs all have very low or no microporosity. The major contribution to total surface area is from external surfaces and is thus predominantly determined by particle size and shape rather than high internal porosity. NM-211 has the highest surface area and micropore volume of all the NMs consistent with particle size observations.

The dustiness results show moderate respirable and inhalable dustiness levels for both NM-211 and NM-212. For NM-213 the dustiness results show very low respirable and inhalable dustiness levels and the index for NM-213 is classified to be at the very low end of dustiness levels.

There is still some ambiguity concerning the redox potential parameter i.e. as to what and how to measure, particularly in a nano-ecotoxicological context. The study investigates the redox potential measurements of CeO_2 dispersions in various liquid media using ORP probe electrode. Although the redox potential values acquired from

ORP electrode may be indicative of the redox state of the entire system it is difficult to quantify the reliability of such measurements.

Photocatalytic activity was measured using anatase TiO_2 as positive control. Results showed that anatase TiO_2, as expected, was the most active photocatalytic material, showing a much higher rate of tri-iodide formation than tests with the CeO_2 NMs. NM-212 has a trend similar to anatase TiO_2, in having the largest absorbance signal in DI water and the smallest when in seawater. For NM-211 and NM-213 the absorbance signals were within a range similar to that of the irradiated blank, i.e. NM-211 and NM-213 were not photocatalytic active. A UV-visible plate reader was used to follow the cumulative production of I^{3-} with varying irradiation time.

5.2 Test Item Preparation

The PROSPEcT dispersion protocol developed during the project was mainly used for dispersion of the nanomaterials but other protocols such as ENPRA and Nanogenotox are also available. In all of these protocols, the NMs are dispersed into the media using sonication. These protocols have been applied for several other nanomaterials in addition to cerium dioxide. The PROSPECT protocol works extremely well to disperse cerium dioxide.

Once the dispersion of the test item has been prepared, analysis should always be performed to ensure dispersion stability, as successful (liquid) sample splitting can only be conducted if a homogeneous dispersion has been achieved, otherwise this will result in a much higher sampling error. Analysis can be performed using a predetermined tool for example light scattering techniques such as Dynamic Light Scattering (DLS) or even optical microscopy. Whatever the choice of characterisation tools chosen, operators must be aware of the limitations posed by the various techniques. For example, in the case of DLS, this tool is not suitable to resolve a broad particle size distribution, as the signal from larger particles can (and usually does) mask the signal of smaller nanoparticles. In order to resolve multi-modal particle distribution, techniques such as Flow Field Flow fractionation that have a separation mechanism element integrated in the analytical tool will be more suitable. In addition to identifying possible errors incurred from sub-sampling steps, stability testing of the dispersion is important for nanoparticle characterisation.

References

Baer D.R. et al, JVST A 31, 050820, (**2013**)

Calzolai, L., Gilliland, D., Garcia, C.P. and Rossi, F. (**2011**) Separation and characterization of gold nanoparticle mixtures by flow-field-flow fractionation. Journal of Chromatography A,1218 (27), pp. 4234-4239.

Cassee, F.R. et al. (**2011**) Exposure, Health and Ecological Effects Review of Engineered Nanoscale Cerium and Cerium Oxide Associated with its Use as a Fuel Additive, Critical Reviews in Toxicology, Vol. 41, No. 3, Pages 213-229.

Cedervall, T., Lynch I., Lindman, S., Berggård, T., Thulin, E., Nilsson, H., Dawson, K.A. and Linse, S. Understanding the nanoparticle–protein corona using methods to quantify exchange rates and affinities of proteins for nanoparticles. The National Academy of Sciences of the USA, PNAS vol. 104 no.7 **2007** pp. 2050-2055.

Chandra Ray, P. et al.; Toxicity and Environmental Risks of Nanomaterials: Challenges and Future Needs. Journal of Environmental Science and Health, Part C, Vol. 27, Issue 1, **2009**, p. 1 – 35.

Chang, H.W. and K. Okuyama, Optical properties of dense and porous spheroids consisting of primary silica nanoparticles. Journal of Aerosol Science, **2002**. 33(12): p. 1701-1720.

Enpra, **2010**, Interim report, *Primary physico-chemical characteristics of engineered nanoparticles used in the ENPRA project*.

HEI - Health Effects Institute, Research Report, **2001**. Evaluation of Human Health Risk from Cerium added to Diesel Fuel.

Hendersen, M.A. et al., Surf. Sci., 526, (**2003**), 1.

Holgado, J.P. et al,, Appl. Surf. Sci., 158, (**2000**), 164,

Jensen, K. A., et al. "Dustiness behaviour of loose and compacted Bentonite and organoclay powders: What is the difference in exposure risk?" Journal of Nanoparticle Research 11.1 (**2009**): 133-46.

Ju-Nam, Y et al.; Manufactured nanoparticles: an overview of their chemistry, interactions and potential environmental implications. Sci Total Environ., **2008**, 400(1-3): p. 396-414.

Linsinger, T., Roebben, G., Gilliland, D., Calzolai, L., Rossi, F., Gibson, N. and Klein, C. Requirements on measurements for the implementation of the European Commission definition of the term 'nanomaterial. European Union, Luxembourg, **2012**. 52 pp. ISBN 978-92-79-25602-8 (pdf) . EUR 25404 EN

Morris J., Willis J., De Martinis D., Hansen, B., Laursen, H., Riego Sintes, J., Kearns, P. and Gonzalez, M. Science policy considerations for responsible nanotechnology decisions. Nature Nanotechnology, 6, **2011**, p. 73-77.

Nowack, B. et al.; Occurrence, behavior and effects of nanoparticles in the environment. Environmental Pollution, Vol 150, Issue 1, **2007**, p. 5-22.

OECD 2010a; ENV-JM-MONO(2009)20-REV-ENG- Guidance Manual for Sponsors, OECD, Paris (**2010**). Available at: http://www.olis.oecd.org/olis/2009doc.nsf/linkto/env-jm-mono%282009%2920.

OECD 2010b; ENV/JM/MONO(2010)46- List of Manufactured Nanomaterials and List of Endpoints for Phase One of the Sponsorship Programme for the Testing of Manufactured Nanomaterials: Revision, OECD, Paris (**2010**). Available at: http://www.olis.oecd.org/olis/2009doc.nsf/linkto/env-jm-mono%282009%2920.

Paparazzo, E. et al., J. Vac. Sci. Technol. A 9(3), (**1991**), 1416

Qiu, L. et al., Appl. Surf. Sci., 252 (2006), 4931

Rama, M.V. et al., J. Electr. Spectrosc. Rel. Phenom., 87, (**1997**), 121

Ratutoiu, N. and Teodorescu, C.M., Digest J. Nanomat and Biostruct., 8(4), (**2013**), 1535.

Roebben, G., Rasmussen, K., Kestens, V., Linsinger, T. P. J., Rauscher, H., Emons, H., Stamm, H. Reference materials and representative test materials: the nanotechnology case. Journal of Nanoparticle Research, Vol. 15, (**2013**) pp. 1455-1468.

Rogers, N., Franklin, N., Apte, S., Batley, G., Angel, B., Lead, J., Baalousha, M. Physico-chemical behaviour and algal toxicity of naoparticulate CeO_2 in freshwater. Environmental Chemistry, 7, (**2010**) p. 50-60.

SCENIHR. Scientific Committee on Emerging and Newly Identified Health Risks (SCENIHR), Opinion on “Risk Assessment of Products of Nanotechnologies”, Brussels, **2009**.

Schneider, T. and Jensen, K.A. "Combined Single-Drop and Rotating Drum Dustiness Test of Fine to Nanosize Powders Using a Small Drum." Annals of Occupational Hygiene 52.1 (**2008**): 23-34.

Singh, C. et al., NM-Series of Representative Manufactured Nanomaterials. Zinc Oxide NM-110, NM-111, NM-112, NM-113. Characterisation and Test Item Preparation. European Union, Luxembourg, EUR 25066 EN (**2011)**. ISBN 978-92-79-22215-3. doi:10.2787/55008

WHO, no year indicated, "Hazard Prevention and Control in the Work Environment: Airborne Dust" available from http://www.who.int/occupational_health/publications/en/oehairbornedust3.pdf

Zhang, F., et al., Cerium oxidation state in ceria nanoparticles studied with X-ray photoelectron spectroscopy and absorption near edge spectroscopy. Surface Science, **2004**. 563(1-3): p. 74-82.

European Commission
EUR 26649 EN – Joint Research Centre – Institute for Health and Consumer Protection

Title: Cerium Dioxide, NM-211, NM-212, NM-213. Characterisation and test item preparation

Author(s): Charanjeet Singh, Steffi Friedrichs, Giacomo Ceccone, Neil Gibson, Keld Alstrup Jensen, Marcus Levin, Heidi Goenga Infante, David Carlander and Kirsten Rasmussen

Luxembourg: Publications Office of the European Union

2014 – 88 pp. – 21.0 x 29.7 cm

EUR – Scientific and Technical Research series – ISSN 1831-9424 (online), ISSN 1018-5593 (print)

ISBN 978-92-79-38308-3 (PDF)
ISBN 978-92-79-38309-0 (print)

doi:10.2788/80203

LB-NA-26649-EN-N

JRC Mission

As the Commission's in-house science service, the Joint Research Centre's mission is to provide EU policies with independent, evidence-based scientific and technical support throughout the whole policy cycle.

Working in close cooperation with policy Directorates-General, the JRC addresses key societal challenges while stimulating innovation through developing new methods, tools and standards, and sharing its know-how with the Member States, the scientific community and international partners.

Serving society
Stimulating innovation
Supporting legislation

doi:10.27788/80203
ISBN 978-92-79-38308-3